Journal of Building Performance Simulation

ISSN: 1940-1493 (Print) 1940-1507 (Online) Journal homepage: https://www.tandfonline.com/loi/tbps20

Phenomenological modelling of phase transitions with hysteresis in solid/liquid PCM

Tilman Barz, Johannn Emhofer, Klemens Marx, Gabriel Zsembinszki & Luisa F. Cabeza

To cite this article: Tilman Barz, Johannn Emhofer, Klemens Marx, Gabriel Zsembinszki & Luisa F. Cabeza (2019): Phenomenological modelling of phase transitions with hysteresis in solid/liquid PCM, Journal of Building Performance Simulation, DOI: 10.1080/19401493.2019.1657953

To link to this article: https://doi.org/10.1080/19401493.2019.1657953

Published online: 05 Sep 2019.

JOURNAL OF BUILDING PERFORMANCE SIMULATION
https://doi.org/10.1080/19401493.2019.1657953

Phenomenological modelling of phase transitions with hysteresis in solid/liquid PCM

Tilman Barz [a], Johannn Emhofer[a], Klemens Marx[a], Gabriel Zsembinszki[b] and Luisa F. Cabeza[b]

[a]AIT Austrian Institute of Technology GmbH, Giefingasse 2, 1210 Vienna, Austria; [b]GREiA Research Group, INSPIRES Research Centre, University of Lleida, Pere de Cabrera s/n, 25001 Lleida, Spain

ABSTRACT

Technical-grade and mixed solid/liquid phase change materials (PCM) typically melt and solidify over a temperature range, sometimes exhibiting thermal hysteresis. Three phenomenological phase transition models are presented which are directly parametrized using data from complete melting and solidification experiments. They predict hysteresis phenomena and are used to calculate effective PCM properties. Two models have already been implemented in commercial building simulation and/or multiphysics software, but not the third novel model. Applications are presented for two commercial PCM: a paraffin, and a salt water mixture with additives. Numerical implementation aspects are discussed, and significant differences in the predicted absorbed and released heat are highlighted when simulating consecutive incomplete phase transitions. The models are linked with energy balance equations to predict recorded PCM temperatures of a thermal energy storage. The cross-validation with data from 26 partial load conditions clearly indicate a superior predictive performance of the novel hysteresis model.

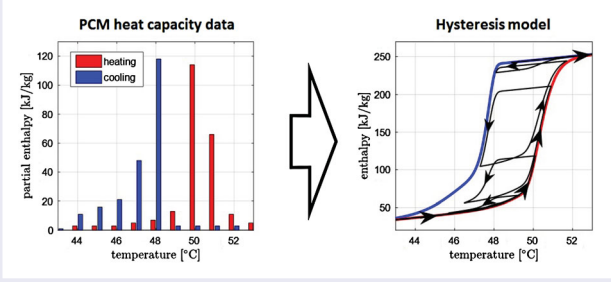

ARTICLE HISTORY
Received 17 January 2019
Accepted 15 August 2019

KEYWORDS
Solid/liquid phase transition; static hysteresis models; identification of PCM properties; incomplete melting and solidification; enthalpy–temperature curves

1. Introduction

The performance of a latent heat thermal energy storage (LHTES) with solid/liquid phase change material (PCM) critically depends on the thermo-physical PCM properties and its phase transition behaviour. Established building performance simulation tools mostly ignore complex phase transition characteristics, relevant for many commercial PCM used in real applications (Al-Saadi and Zhai 2013). A major shortcoming of these simulation tools is the lack of suitable models for the description of thermal hysteresis (Goia, Chaudhary, and Fantucci 2018). Thermal hysteresis effects are complex in nature. They are normally induced by supercooling which is caused by complex nucleation and crystal growth mechanisms. Corresponding mechanistic macroscopic modelling approaches for PCM can be found e.g. in Ziskind (2014) and Uzan et al. (2017). Experimental analysis of hysteresis effects are presented e.g. in Diaconu, Varga, and Oliveira (2010).

In contrast to the mechanistic modelling approach for the analysis of hysteresis in the solid/liquid phase transition of PCM, this contribution follows a purely phenomenological (data-based) approach without consideration of physical processes inside the PCM. Accordingly, the following definition is used (Barz and Sommer 2018):

Definition: (Hysteresis during temperature-induced phase transitions of solid/liquid PCM) The term *hysteresis* is used to indicate that different PCM state parameters, i.e. values of enthalpy h or phase fraction ξ, can be found for the same temperature value T, depending on the direction of change of T, and possibly also on the rate of change of T.

Following the phenomenological approach for modelling thermal hysteresis, Goia, Chaudhary, and Fantucci (2018) used two different building simulation software (EnergyPlus™: and Wufi®Pro/Plus), to implement different phenomenological phase transition models which are defined by enthalpy–temperature curves. These curves are derived from the PCM heat capacity and phase transition data obtained from various calorimetric methods, including differential scanning calorimetry (DSC) for complete melting and solidification (Goia, Chaudhary,

CONTACT Tilman Barz tilman.barz@ait.ac.at AIT Austrian Institute of Technology GmbH, Giefingasse 2, 1210 Vienna, Austria

and Fantucci 2018). The models implement enthalpy–temperature curves which correspond to the curve for complete melting, complete solidification, or an average between both curves. The experimental validation of these models with temperature data from various PCM during consecutive complete and incomplete phase transitions revealed adequate simulation results for PCM with low hysteresis during complete phase transitions. However, high inaccuracies were found for incomplete transitions and PCM showing significant hysteresis effects (Goia, Chaudhary, and Fantucci 2018). The same approach for identification of complete transition models and their use for modelling of complete phase transitions was followed by Frei (2016), Virgone and Trabelsi (2016), Michel et al. (2017), Biswas et al. (2018) and Hu and Heiselberg (2018) using COMSOL Multiphysics®, and by Diaconu and Cruceru (2010), Moreles, Huelsz, and Barrios (2018), and Gasia et al. (2018) using in-house simulation code.

An alternative phenomenological modelling approach for the consideration of hysteresis and varying enthalpy–temperature relationship was proposed by Gowreesunker, Tassou, and Kolokotroni (2012), Gowreesunker and Tassou (2013) and Kumarasamy et al. (2016, 2017). The so called 'source term' approach uses a heat source term in the PCM energy balance equation model to represent the latent heat during phase change. This modelling technique corresponds to the default solidification/melting model in ANSYS Fluent (Kumarasamy et al. 2017). The authors use DSC heat capacity data obtained for complete melting and for complete solidification. From this data two different models for the latent heat evolution with temperature are derived. This approach is also restricted to the analysis of hysteresis effects for complete melting and solidification experiments.

All mentioned models realize (or track) enthalpy–temperature transition curves identified either for complete melting, or for complete solidification. According to the naming convention used in NRGsim, which is a custom sub-routine developed for EnergyPlus™ (NRGSIM 2018), these models are referred to as 'curve track' models. For PCM mixtures, including technical-grade PCM, the main drawback of the 'curve track' model is its poor performance when applied to predict phase transition behaviour with hysteresis for partial melting and solidification, see e.g. Diaconu and Cruceru (2010), Moreles, Huelsz, and Barrios (2018), Gasia et al. (2018), Goia, Chaudhary, and Fantucci (2018). For this reason, based on experimental findings, an extension of the 'curve track' model was proposed by Bony and Citherlet (2007) which realizes a switch from one transition curve to the other for direction changes in the temperature during incomplete phase transitions, the so called 'curve switch' model. This approach was taken up by Rose et al. (2009), and was also implemented in NRGsim.

Diaconu, Varga, and Oliveira (2010) found experimentally that the hysteresis magnitude decreased in the case of temperature cycling inside the PCM phase transition temperature range. They also found that the temperature history influences the enthalpy values (Diaconu, Varga, and Oliveira 2010). The same behaviour was found by Delcroix, Kummert, and Daoud (2017).

An alternative hysteresis model, originally examined by Ivshin and Pence (1994) in the context of temperature-induced phase transitions, was applied recently to model hysteresis phenomena in PCM for thermal energy storages by Barz and Sommer (2018). To take up the naming convention established in the documentation of NRGsim, in the following this model is referred to as 'curve scale' model. The 'curve scale' model accounts for different hysteresis magnitudes for cycles within the phase transition temperature range and makes use of the temperature history. A variant of the 'curve scale' model was also proposed by Delcroix (2015); Delcroix, Kummert, and Daoud (2017) and implemented in TRNSYS. First studies with the 'curve scale' model, and comparison with experimental temperature data recorded in a LHTES showed convincing results in terms of prediction of hysteresis effects during partial charging and discharging operation (Barz and Sommer 2018).

This contribution continues the work started by Barz and Sommer (2018) on the application of the 'curve scale' model for PCM and presents a systematic comparative analysis of the three different hysteresis models, namely the 'curve track', 'curve switch' and the 'curve scale' models. The models are applied to predict temperature-induced phase transitions in technical-grade solid/liquid PCM mixtures. They are rate-independent and thus, predict equilibrium states of the PCM. These states characterize the PCM solid, liquid or mushy state.[1] The phase transition models might be used to predict thermo-physical properties, e.g. PCM enthalpies. They can be applied for the numerical solution of heat transfer problems in PCM.

For the 'curve track' and 'curve switch' hysteresis models implementations are available in commercial building simulation and/or multiphysics software. For the 'curve scale' hysteresis model proposed in this contribution no such implementation exists. The purpose of this contribution is firstly, to provide a detailed analysis on the numerical implementation and performance of all three models, and secondly, to present a quantitative assessment of the predictive performance of the models. A special focus is on their use for simulating incomplete phase transitions (during consecutive partial melting and solidification) as especially relevant during partial load operation of LHTES. Both points have not been presented before.

Sections 2 and 3 introduce the common assumptions and modelling approaches for all three hysteresis models. All models assume that the PCM melts and solidifies within a phase transition temperature range with coexisting phases. Section 2 introduces the two-phase modelling approach, where the (liquid mass) phase fraction is used as the characteristic PCM state parameter. For complete phase transitions, i.e. complete melting or complete solidification, the evolution of the phase fraction is modelled by simple functions which depend on the PCM temperature (Section 2.1). These phase transition functions are used to predict all PCM properties within the phase transition temperature range (Section 2.2). The identification of phase transition functions from heat capacity data of two commercial PCM is discussed in Section 3. The heat capacity data shows temperature hysteresis. Therefore different phase transition functions are identified, one for complete melting and one for complete solidification. Section 4 presents a mathematical description of the three hysteresis models together with a discussion on their numerical implementation and main characteristics. All three hysteresis models are completely defined by

the phase transition functions identified in Section 3. The models differ in the prediction of hysteresis effects during incomplete phase transitions. This is discussed in Section 5, where simulation studies are carried out for two commercial PCM. In Section 5.1, temperature-induced phase transitions are computed for consecutive incomplete melting and solidification. In Section 5.2, enthalpy–temperature curves are computed to discuss differences of the hysteresis models in terms of predicted absorbed and released heat. An application of the hysteresis models to simulate PCM temperatures measured inside of a LHTES is presented in Section 6. The hysteresis models are linked with a numerical energy balance equation model of the LHTES (Section 6.1). The hysteresis model parameters are identified from PCM temperature measurements during complete charging and discharging storage operation (Section 6.2). In Section 6.3, predicted PCM temperatures are compared with experimental data from 26 partial load (charging and discharging) operations. The results clearly indicate a superior predictive performance of the 'curve scale' model proposed in this contribution. The numerical performance is discussed in Section 6.4. Finally, Section 7 gives a discussion and conclusions.

2. The two-phase model

Phase transitions are modelled based on the general assumption, that the overall structure of the PCM can be approximated by two phases, a solid and a liquid phase. For PCM mixtures, including technical-grade PCM as available from commercial manufacturers, the phase change does not occur at an exact temperature, but rather within a specific temperature range. This means that it is assumed that the two phases coexist during solid/liquid phase transition and allows to approximate the overall structure of the PCM by one characteristic parameter $\xi \in [0, 1]$,

$$\xi := \frac{m^l}{m^l + m^s} \tag{1}$$

denoting the (liquid mass) phase fraction, and m^s and m^l are the masses of solid and liquid phase, respectively.

2.1. Phase transition functions for complete melting/solidification

Most simple models for the phase transition (between solid with $\xi = 0$ and liquid with $\xi = 1$) assume that the phase fraction is a direct function of temperature: $\xi := \xi(T)$. In the following $\xi(T)$ is referred to as '(phase) transition function'. These functions directly relate temperature T to phase fraction ξ. Moreover, since ξ ranges from 0 to 1 and monotonously increases with rising temperature, these functions

- must be injective functions, and
- must realize a smooth transition from $\xi = 0$ to $\xi = 1$.

Thus, cumulative distribution functions seem convenient to be used as 'transition function':

$$\xi(T) := \int_{-\infty}^{T} \phi(\tau)\,\mathrm{d}\tau \quad \text{with} \int_{-\infty}^{\infty} \phi(\tau)\,\mathrm{d}\tau = 1 \tag{2}$$

In Equation (2), $\phi(T)$ is a (continuous) probability distribution function (PDF), or simply distribution function. Accordingly, $\xi(T)$ is then the corresponding cumulative distribution function. Distribution functions are also convenient as they can be parametrized by a relatively small number of location and shape parameters. This is especially useful when fitting phase transition models to experimental data by numerical solution of a non-linear regression problem. Moreover, independent of the selected values of location and shape parameters, distribution functions $\phi(T)$ always preserve the integral value of one. Therefore scaling of these functions is straightforward and these 'transition functions' can be directly used to model changes of any thermo-physical material properties which are affected by phase change, such as heat capacity, enthalpy, density, etc.

In this contribution, the transition functions $\xi(T)$ are modelled using extreme value type I distribution functions, also referred to as the Gumbel (Minimum and Maximum) distributions NIST/SEMATECH (2015). In contrast to the Gaussian PDF, these PDF have a closed (analytic) form of the respective cumulative distribution function and thus, are easier to implement in different software environments. They are also convenient for representing asymmetric peaks. The Gumbel Minimum distribution is based on the smallest extreme of a distribution while the Gumbel Maximum distribution is based on the largest extreme. The formula for the Gumbel distributions reads:

$$\phi^G(T;\mu,\beta,\kappa) = \frac{1}{\beta}\,\exp\left(\kappa\frac{T-\mu}{\beta}\right)\exp\left(-\exp\left(\kappa\frac{T-\mu}{\beta}\right)\right) \tag{3}$$

where T is the temperature in K, and μ, β are the respective location and shape parameters, and $\kappa = 1$ in the Minimum, and $\kappa = -1$ in the Maximum case. Secondly, because of the higher shape flexibility an adapted Weibull density function (NIST/SEMATECH 2015) is also considered (adaptation, mirrored around μ):

$$\phi^W(T;\mu,\gamma,\alpha) = \begin{cases} \dfrac{\gamma}{\alpha}\left(-\dfrac{T-\mu}{\alpha}\right)^{\gamma-1}\exp\left(\left(\dfrac{T-\mu}{\alpha}\right)^{\gamma}\right), & T < \mu \\ 0, & T \geq \mu \end{cases} \tag{4}$$

where μ, γ, α are location and shape parameters.

In addition, it is sometimes useful to extend the models by a superposition of distribution functions $\mathcal{D} \in \{G, W\}$:

$$\phi^{\Sigma} = \sum_{i=1}^{n} w_i \phi_i^{\mathcal{D}} \tag{5}$$

each $\phi_i^{\mathcal{D}}$ with its own parameters μ_i, β_i, κ_i, γ_i, α_i, and with $\kappa_i \in \{-1, 1\}$. Moreover, $w_i > 0$ is a weighting parameter with $\sum_{i=1}^{n} w_i = 1$.

2.2. Two-phase material property models

For the here considered PCM mixtures, including technical-grade PCM, it was assumed that solid and liquid phases coexist within the phase transition temperature range. Therefore, within this range the PCM thermo-physical properties are modelled by

a superposition of contributions from solid and liquid PCM properties. This superposition gives then so called 'effective' PCM properties.

2.2.1. Effective specific heat capacity

A two-phase model for the effective specific heat capacity $\tilde{c}$ of the PCM is given by a linear superposition of terms for liquid and solid specific heat capacity (c_p^l and c_p^s, respectively) as well as the specific phase transition enthalpy (Δh_t) released or absorbed in the phase transition region (Gaur and Wunderlich 1981):

$$\tilde{c} := \xi c_p^l + (1-\xi)c_p^s + \frac{d\xi}{dT}\Delta h_t \tag{6}$$

Note that in Equation (6), ξ is the phase transition function and depends on temperature, i.e. $\xi = \xi(T)$. Possible functions for ξ and its derivative $d\xi/\mathrm{d}T$ were proposed in Section 2.1, where ξ is modelled by a cumulative distribution function and $d\xi/\mathrm{d}T$ is its corresponding distribution function ϕ, see (2).

2.2.2. Effective enthalpy

Enthalpy–temperature relations $h(T)$ are obtained by integration of Equation (6):

$$\begin{aligned} h(T) - h(T_{\text{ref}}) &= \int_{T_{\text{ref}}}^{T} \tilde{c}(\tau)\,\mathrm{d}\tau \\ &= \int_{T_{\text{ref}}}^{T} \left(\xi(\tau)c_p^l + (1-\xi(\tau))c_p^s\right)\,\mathrm{d}\tau \\ &\quad + \Big(\xi(T) - \xi(T_{\text{ref}})\Big)\Delta h_t \end{aligned} \tag{7}$$

It is noted that, for convenience only, in Equation (7) c_p^l and c_p^s are assumed constant. Moreover, it seems reasonable to assume that T_{ref} is much smaller than the temperatures defining the phase transition temperature range. In this case, in Equation (7) $\xi(T_{\text{ref}}) = 0$.

2.2.3. Effective density and thermal conductivity

In the same way as for the liquid and solid specific heat capacity in Equation (6), all other PCM properties can also be modelled by a linear superposition of terms for liquid and solid PCM properties. The transition function $\xi(T)$ is used to compute their weights. The effective density and thermal conductivity models read:

$$\tilde{\rho} := \xi\rho^l + (1-\xi)\rho^s \tag{8}$$

$$\tilde{\lambda} := \xi\lambda^l + (1-\xi)\lambda^s \tag{9}$$

3. Identification of phase transition functions from heat capacity data

The phase transition functions in Section 2.1, i.e. functions for $\xi := \xi(T)$, can be (indirectly) identified by fitting the effective specific heat capacity model Equation (6) to heat capacity data of the PCM (Barz and Sommer 2018). The fitting is performed by numerical solution of a non-linear regression problem. The fitting parameters are c_p^s, c_p^l, Δh_t as well as the parameters of the selected phase transition functions ϕ^G and/or ϕ^W, μ_i, β_i, κ_i, γ_i, α_i and w_i in Equations (3)–(5).

3.1. Rubitherm PCM RT64HC

Results are discussed for Rubitherm PCM RT64HC. Heat capacity data provided by the PCM manufacturer is used, see Rubitherm GmbH (2018). The data (partial enthalpies) were recorded during heating and cooling using a three-layer-calorimeter. Results from fitting the effective specific heat capacity model to the manufacturer data are presented in Figure 1. Two different phase transition functions were identified, one for heating (solid-to-liquid transition function $\xi^{\text{s}\to\text{l}}$) and one for cooling (liquid-to-solid transition function $\xi^{\text{l}\to\text{s}}$). For each, a superposition of two Gumbel Minimum distribution functions (ϕ_1^G and ϕ_2^G in Equation (5)) were fitted. The identified regression parameters of the distribution functions for heating are: $\mu_1 = 334.1$, $\beta_1 = 0.86$, $\kappa_1 = 1$, $w_1 = 0.06$, and $\mu_2 = 337.4$, $\beta_2 = 0.57$, $\kappa_2 = 1$, $w_2 = 0.94$. The parameters for cooling are: $\mu_1 = 334.1$, $\beta_1 = 0.7$, $\kappa_1 = 1$, $w_1 = 0.41$, and $\mu_2 = 337.3$, $\beta_2 = 0.4$, $\kappa_2 = 1$, $w_2 = 0.59$. The estimated specific heat capacity and phase transition enthalpy values (same for heating and for cooling) are: $c_p^s = c_p^l = 2.4\,\text{kJ/kg/K}$ and $\Delta h_t = 221.0\,\text{kJ/kg}$.

According to the manufacturer data sheet the heat storage capacity in the temperature range from 57°C to 72°C, is 250 kJ/kg (±7.5%). Using the estimated values for c_p and Δh_t above, the estimated heat storage capacity in the same temperature range is 257 kJ/kg. Thus, the estimated values seem reasonable.

The quality of the parameter estimates is assessed by an identifiability analysis. It is a local analysis based on the condition of the sensitivity matrix at the solution of the regression problem, for details see López Cárdenas et al. (2015). For heating, the condition number of the sensitivity matrix is 11,669. This value exceeds the maximum threshold of 1000 and diagnoses an ill-conditioned matrix. However, none of the singular values is very close to zero (values between 5.14 and 59,984) and the collinearity index is 0.195 and below its maximum threshold of 15. Therefore the problem can be considered rank-deficient. For cooling, the condition number is 4035 diagnosing ill-conditioning. However, the singular values are well above zero (between 11.9 and 48,050) and the collinearity index is with 0.084 below the critical threshold. Thus, the problem can also be considered rank-deficient. It can be concluded that for both, heating and cooling, the estimated parameter values are not severely affected by the ill-conditioning of the sensitivity matrix.

The analysis also reveals that for heating only four out of seven parameters can be reliably estimated from the heat capacity data, while for cooling five out of seven parameters can be reliably estimated. The ranking of parameters regarding their linear independence and sensitivity yields the following decreasing order for heating: μ_2, μ_1, Δh_t, β_2, c_p, w_1, β_1, and for cooling: μ_2, μ_1, Δh_t, w_1, β_2, β_1, c_p. (Note that $w_2 = 1 - w_1$, it is not an estimated parameter.) Thus, the location parameters of the distribution functions μ_i and the phase transition enthalpy Δh_t can be most reliably estimated, in contrast to the shape parameters of the distribution functions. This is to be expected considering the relatively small number of data points which do not give clear information on all peak shapes. The analysis shows that the number of parameters which can be reliably estimated is greater (plus one) for cooling as for heating. This seems also reasonable as the cooling data shows the superposition of

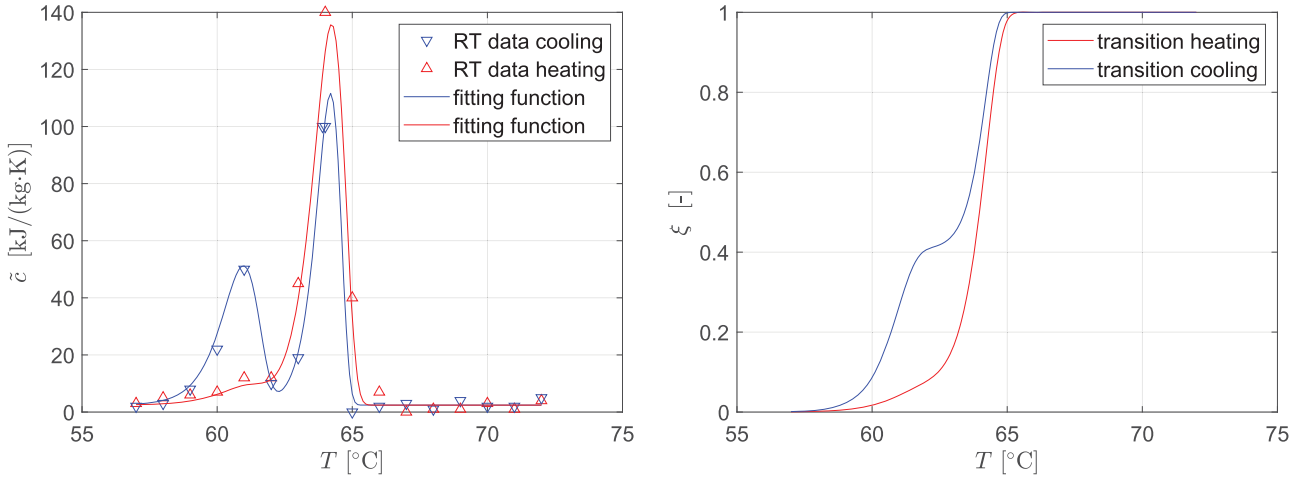

Figure 1. Fitting heat capacity data from Rubitherm RT64HC. Data for heating and cooling is fitted individually using Gumbel distributions. Left: fitting functions for effective specific heat capacity. Right: corresponding phase transition functions.

two peaks more clearly compared with the heating data, see Figure 1 left.

3.2. Rubitherm PCM SP50

Phase transition functions are identified from heat capacity data taken from Rubitherm PCM SP50 material data sheet, shown in Figure 2. The data (partial enthalpies) were recorded during heating and cooling using a three-layer-calorimeter Rubitherm GmbH (2018). Again, two different phase transition functions were identified, $\xi^{s\to l}$, $\xi^{l\to s}$. For each, a superposition of two Gumbel distribution functions (ϕ_1^G and ϕ_2^G in Equation (5)) were fitted. The identified regression parameters of the distribution functions for heating are: $\mu_1 = 323.4$, $\beta_1 = 0.48$, $\kappa_1 = -1$, $w_1 = 0.78$, and $\mu_2 = 323.2$, $\beta_2 = 0.99$, $\kappa_2 = 1$, $w_2 = 0.22$. The parameters for cooling are: $\mu_1 = 319.0$, $\beta_1 = 0.96$, $\kappa_1 = 1$, $w_1 = 0.21$, and $\mu_2 = 320.9$, $\beta_2 = 0.31$, $\kappa_2 = 1$, $w_2 = 0.79$. The estimated specific heat capacity and phase transition enthalpy values (same for heating and for cooling) are: $c_p^s = c_p^l = 2.6$ kJ/kg/K and $\Delta h_t = 193.1$ kJ/kg.

According to the manufacturer data sheet the heat storage capacity in the temperature range from 40°C to 55°C is 220 kJ/kg (±7.5%). Using the estimated values for c_p and Δh_t above, the estimated heat storage capacity in the same temperature range is 232.1 kJ/kg. Thus, the estimated values seem reasonable.

Similarly as for RT64HC the identifiability analysis diagnoses rank-deficient regression problems for both heating and cooling. For heating, the condition number is 47,245, the singular values are between 1.16 and 54,910, and the collinearity index is 0.86. For cooling, the condition number is 38,498, the singular values are between 4.1 and 157,058, and the collinearity index is 0.25. In conclusion, for both, heating and cooling, the estimated parameter values are not severely affected by the ill-conditioning of the sensitivity matrix.

For heating only three out of seven parameters can be reliably estimated. For cooling only two out of seven parameters can be reliably estimated. The ranking of parameters regarding their linear independence and sensitivity yields the following decreasing order for heating: μ_1, μ_2, Δh_t, β_1, c_p, β_2, w_1, and for cooling:

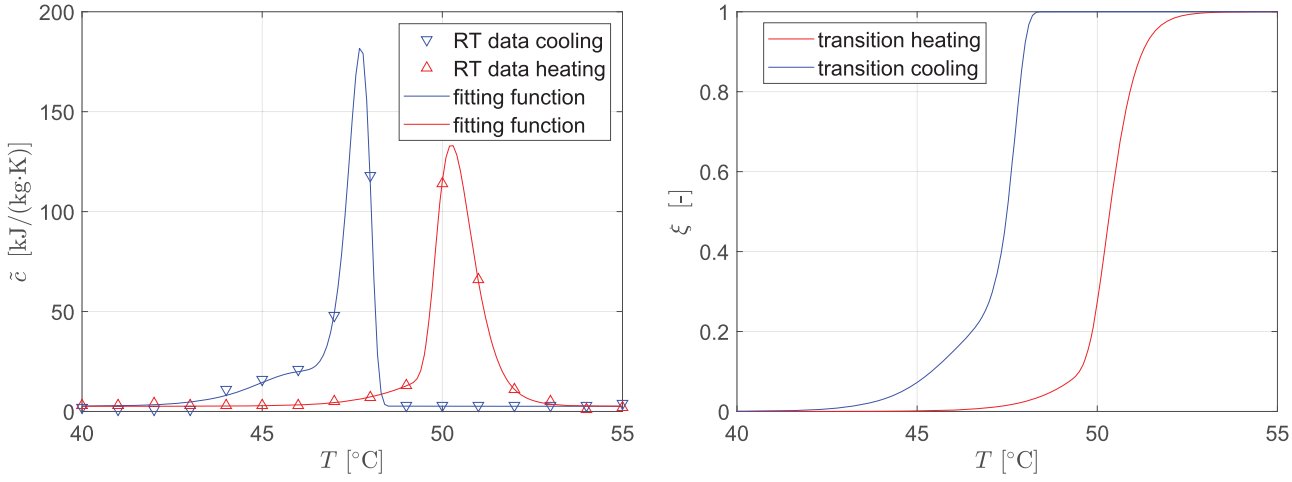

Figure 2. Fitting heat capacity data from Rubitherm SP50. Data for heating and cooling is fitted individually using Gumbel distributions. Left: fitting functions for effective specific heat capacity. Right: corresponding phase transition functions.

μ_2, μ_1, Δh_t, β_2, w_1, c_p, β_1. The results are in line with results obtained for RT64HC.

4. Hysteresis models

In Section 3, for each PCM different phase transition functions were identified from heat capacity data. These are the solid-to-liquid transition function $\xi^{s\to l}$ for complete melting, and the liquid-to-solid transition function $\xi^{l\to s}$ for complete solidification. Within the phase transition region defined by $\xi^{s\to l}$ and $\xi^{l\to s}$, two different phase fraction values can be found for the same temperature value. This phenomenon is known as hysteresis.

In the following, different phenomenological modelling approaches which account for hysteresis in the phase transition of PCM are considered: the 'curve track', the 'curve switch' and the 'curve scale' model. Their mathematical description is presented in Sections 4.1–4.3. All three hysteresis models predict the same phase transition behaviour during complete melting or solidification using corresponding transition functions: one where the PCM undergoes complete solid-to-liquid phase change (this one is described by $\xi^{s\to l}$), and another where the PCM undergoes complete liquid-to-solid phase change (this one is described by $\xi^{l\to s}$). $\xi^{s\to l}$ is used if the material has passed the temperature for complete solidification T^{min} ($T < T^{min}$), while $\xi^{l\to s}$ is used if the material has passed the temperature for complete melting T^{max} ($T > T^{max}$). These temperatures (T^{min} and T^{max}) define the limits of the phase transition temperature range, see Figure 3 for an illustration.

It is noted that all three hysteresis models are phenomenological models. Thus, they can be directly parametrized based on heat capacity data from complete melting and solidification experiments, as discussed e.g. by Goia, Chaudhary, and Fantucci (2018) and Barz and Sommer (2018) for data obtained from DSC.

Furthermore, all presented models are rate-independent (static), therefore the models and the predicted liquid phase fractions do not depend on applied heating or cooling rates. In other words, if a simulation of PCM melting behaviour during heating is always started with the same initial conditions (and history), then, for any final temperature the predicted liquid fractions of molten PCM will be the same regardless of the applied heating rate. This also means that increased heating (or cooling) rates will directly lead to faster melting (or solidification), i.e. faster increases (or decreases) in the liquid phase fraction. Furthermore, if the temperature is held constant, also the phase fraction stays constant.

4.1. 'Curve track' hysteresis model for complete phase transitions

The 'curve track' model, as implemented in COMSOL and NRGsim, is completely defined by the phase transition functions $\xi^{s\to l}$ and $\xi^{l\to s}$, and two additional parameters, namely the minimal (T^{min}) and maximal (T^{max}) temperature of the phase transition range. The model is able to predict phase transitions where the PCM undergoes either complete solid-to-liquid phase change described by $\xi^{s\to l}$, or complete liquid-to-solid phase change described by $\xi^{l\to s}$, see Figure 3. The model does not account for incomplete phase transitions. This means that switches between heating and cooling operation while the material is still within the phase transition range (phase transition is not completed), do not result in a change of the phase transition curve, see Figure 4 for an illustration.

The 'curve track' hysteresis model describes the evolution of the phase fraction as response to positive or negative changes in temperature T from a starting value T_0 to the final value T_f:

$$\xi(T) := \xi^{s\to l}(T) \quad \text{if} \quad T_0 = T^{min} \tag{10a}$$

$$\xi(T) := \xi^{l\to s}(T) \quad \text{if} \quad T_0 = T^{max} \tag{10b}$$

Together with the model in Equation (10), the following two conditions are monitored. If a condition is fulfilled an event is triggered, and the final variable T_f is set, and the model is

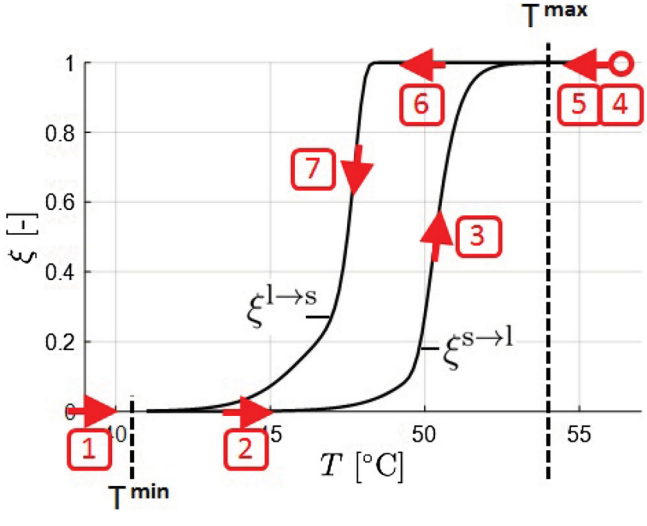

Figure 3. Phase transitions for the 'curve track', 'curve switch' and 'curve scale' model for complete melting (heating) and subsequent solidification (cooling). Numbers indicate the sequence, arrows the direction of temperature changes.

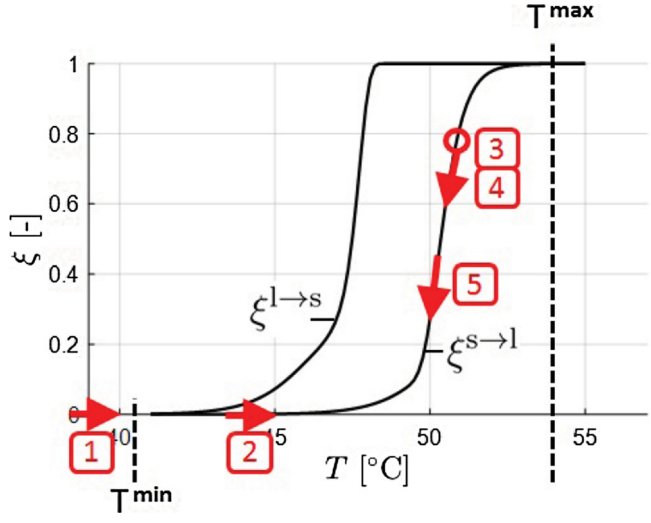

Figure 4. Phase transitions for the 'curve track' model for incomplete melting (heating) and subsequent solidification (cooling). Numbers indicate the sequence, arrows the direction of temperature changes.

switched:

$$\text{if any} \quad \begin{cases} T = T^{\min} \\ T = T^{\max} \end{cases} \quad \text{set} \quad T_f = T \quad \text{and switch model.} \tag{11}$$

In other words, if the value of T meets an active condition, i.e. $T = T^{\max}$ in Equation (10a), or $T = T^{\min}$ in Equation (10b), then T has reached its final value T_f. The model is switched and the process is restarted by setting $T_0 = T_f$. As long as the active condition is not met there is no change of the model.

Note that in Equation (11) events are triggered only when approaching $T^{\min}$ from $T > T^{\min}$, and $T^{\max}$ from $T < T^{\max}$, respectively.

4.2. 'Curve switch' hysteresis model for incomplete phase transitions

The 'curve switch' model adopts an approach proposed by Bony and Citherlet (2007), where incomplete phase transitions are modelled by a straight line between the enthalpy–temperature curves for complete melting ($h^{\mathrm{s}\to\mathrm{l}}(T)$) and for complete solidification ($h^{\mathrm{l}\to\mathrm{s}}(T)$). Following this connecting line realizes the so called 'curve switch'.

While Bony and Citherlet (2007) use $h(T)$ for the characterization of phase transitions, in this work $\xi(T)$ is used. It is noted that there is a direct relation between $h(T)$ and $\xi(T)$ by the PCM properties $c_p^l, c_p^s, \Delta h_t$. Thus, the 'curve switch' modelling approach can be directly applied to the $\xi(T)$ hysteresis model of this contribution.

From the graph shown in Bony and Citherlet (2007, Figure 5) it can be seen that piece-wise linear functions are used to parametrize $h^{\mathrm{s}\to\mathrm{l}}(T)$ and $h^{\mathrm{l}\to\mathrm{s}}(T)$. According to Bony and Citherlet (2007), the slope of the connecting line is the same as the slope of the $h(T)$ curve outside of the phase transition temperature range. This means that the slope is defined by the specific heat capacity, i.e. $\mathrm{d}h/\mathrm{d}T = c_p$. Accordingly, in the $\xi(T)$ phase transition model of this contribution the slope of the connecting line is zero, i.e. $d\xi/\mathrm{d}T = 0$. In other words, the phase fraction does not change when following the connecting line during a 'curve switch'. It is noted that Rose et al. (2009) propose an alternative version of the 'curve switch' model where the connecting line is horizontal (in the enthalpy–temperature plot).

The 'curve switch' model is completely defined by the phase transition functions $\xi^{\mathrm{s}\to\mathrm{l}}$, $\xi^{\mathrm{l}\to\mathrm{s}}$ and $T^{\min}$, $T^{\max}$. For complete melting and solidification the 'curve switch' model produces the same results as the 'curve track' model, see Figure 3. The characteristic phase transitions for incomplete melting and solidification are depicted in Figure 5. The evolution of the phase fraction as response to positive or negative changes in temperature T from a starting value T_0 to the final value T_f is modelled as

$$\xi(T) := \xi^{\mathrm{s}\to\mathrm{l}}(T) \quad \text{if} \quad T_0 = T^{\min} \tag{12a}$$

$$\xi(T) := \xi^{\mathrm{l}\to\mathrm{s}}(T) \quad \text{if} \quad T_0 = T^{\max} \tag{12b}$$

$$\xi(T) := \text{const.} \quad \text{if} \quad T^{\min} < T_0 < T^{\max} \tag{12c}$$

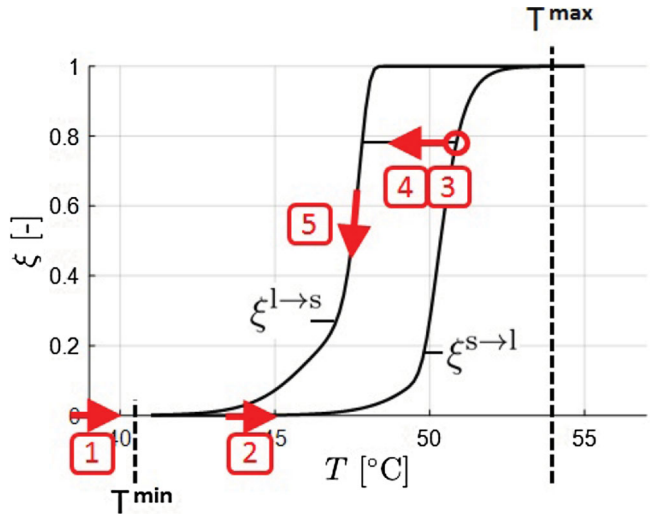

Figure 5. Phase transitions for the 'curve switch' model for incomplete melting (heating) and subsequent solidification (cooling). Numbers indicate the sequence, arrows the direction of temperature changes.

The following conditions are monitored. If a condition is fulfilled an event is triggered, and the variable T_f is set:

$$\text{if any} \quad \begin{cases} T = T^{\min} \\ T = T^{\max} \end{cases} \quad \text{set} \quad T_f = T \quad \text{and} \quad \begin{cases} \text{switch to complete} \\ \text{transition model.} \end{cases} \tag{13a}$$

In the same way as for the 'curve track' model, the conditions in Equation (13a) activate either model Equation (12a) or Equation (12b). Consequently, the phase fraction follows the path for complete phase transition defined by $\xi^{\mathrm{s}\to\mathrm{l}}(T)$ and $\xi^{\mathrm{l}\to\mathrm{s}}(T)$. In addition, if a change in the sign of the temperature rate occurs while the phase transition is still not completed, an event is triggered and model Equation (12c) is activated:

$$\text{while} \quad \begin{cases} T^{\min} < T < T^{\max} \quad \text{and} \\ T_0 = T^{\min} \quad \text{or} \quad T_0 = T^{\max} \end{cases} \quad \text{if} \quad \operatorname{sgn}\left(\frac{\mathrm{d}T}{dt}\right) = 0 \quad \text{set} \quad T_f = T \quad \text{and} \quad \begin{cases} \text{switch to} \\ \text{connecting line.} \end{cases} \tag{13b}$$

Finally, the following conditions are relevant when following the connecting line between $\xi^{\mathrm{s}\to\mathrm{l}}$ and $\xi^{\mathrm{l}\to\mathrm{s}}$, i.e. when model Equation (12c) is active:

$$\text{while} \quad T^{\min} < T_0 < T^{\max} \quad \text{if any} \quad \begin{cases} \xi(T) = \xi^{\mathrm{s}\to\mathrm{l}}(T) & \text{set} \quad T_f = T^{\min} \\ \xi(T) = \xi^{\mathrm{l}\to\mathrm{s}}(T) & \text{set} \quad T_f = T^{\max} \end{cases} \quad \text{and} \quad \begin{cases} \text{switch to complete} \\ \text{transition model.} \end{cases} \tag{13c}$$

This means that model Equation (12c) is active as long as the phase fraction value $\xi(T)$ has not reached either of the two corresponding transition function values $\xi^{\mathrm{s}\to\mathrm{l}}(T)$ and $\xi^{\mathrm{l}\to\mathrm{s}}(T)$, i.e.

the 'curve switch' has not been completed. It is noted that during a 'curve switch' direction changes in the temperature rate do not trigger an event and do not lead to a model switch. It is also noted that, for convenience of implementation, in Equation (13c) T_f is set directly to $T^{\min}$ or to $T^{\max}$ to indicate that the next model to be used is either Equation (12a) or Equation (12b), respectively. Thus, after the following restart and after setting $T_0 = T_f$, T_0 is not necessarily equal to the true starting value T_0. Instead, T_0 is rather used as a flag to store information on the actual model to be used.

4.3. 'Curve scale' hysteresis model for incomplete phase transitions

The 'curve scale' hysteresis model proposed is completely defined by the phase transition functions $\xi^{\mathrm{s}\to\mathrm{l}}$ and $\xi^{\mathrm{l}\to\mathrm{s}}$. In the same way as for the 'curve track' model, it switches between two models. The decision on the model to be used depends on the sign of the temperature rate. This means that there exists one model for heating with $\operatorname{sgn}(\mathrm{d}T/\mathrm{d}t) > 0$, and one model for cooling with $\operatorname{sgn}(\mathrm{d}T/\mathrm{d}t) < 0$.

As the name suggests, after changes in the direction of the temperature rate during incomplete phase transitions, both models scale the transition functions. The scaling depends on the pair of values (T_0, ξ_0) at the last switching point, with $\xi_0 = \xi(T_0)$.

It is noted that Delcroix (2015) proposes a variant of the 'curve scale' model based on experimental findings using enthalpy–temperature curves. Accordingly, during partial phase transitions after changing from heating to cooling the process follows an enthalpy–temperature curve placed between the curves for complete phase transitions.

For complete melting and solidification the 'curve scale' model produces the same results as the 'curve track' and the 'curve switch' model, see Figure 3. The characteristic phase transitions for incomplete melting and solidification are depicted in Figure 6. The evolution of the phase fraction as response to a monotonous change in temperature T from a starting value T_0 to the final value T_f is modelled as

$$\xi(T) := 1 - \frac{1-\xi(T_0)}{1-\xi^{\mathrm{s}\to\mathrm{l}}(T_0)} \cdot \left(1-\xi^{\mathrm{s}\to\mathrm{l}}(T)\right) \quad \text{if} \quad \operatorname{sgn}\left(\frac{\mathrm{d}T}{dt}\right) \geq 0 \tag{14a}$$

$$\xi(T) := \frac{\xi(T_0)}{\xi^{\mathrm{l}\to\mathrm{s}}(T_0)} \cdot \xi^{\mathrm{l}\to\mathrm{s}}(T) \quad \text{if} \quad \operatorname{sgn}\left(\frac{\mathrm{d}T}{dt}\right) < 0 \tag{14b}$$

where $\xi(T_0) = \xi_0$ denotes the initial phase fraction at temperature T_0.

The following condition is monitored. If the condition is fulfilled an event is triggered, and the final variables T_f and ξ_f are set:

$$\text{if} \quad \operatorname{sgn}\left(\frac{\mathrm{d}T}{dt}\right) = 0 \quad \text{set} \quad \begin{cases} T_f = T \\ \xi_f = \xi \end{cases} \quad \text{and switch model.} \tag{15}$$

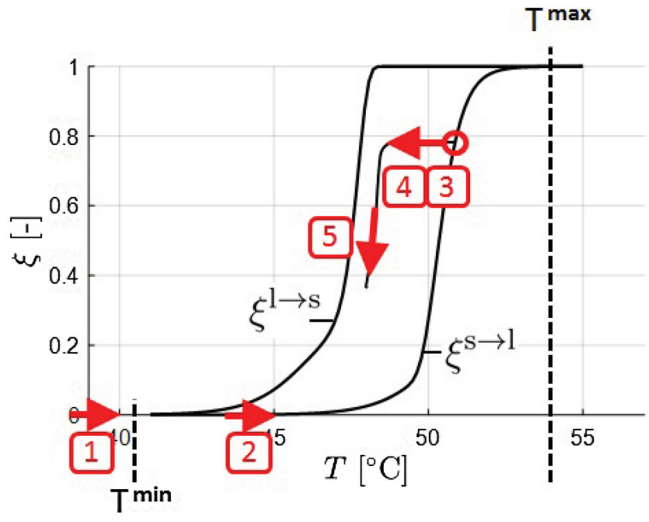

Figure 6. Phase transitions for the 'curve scale' model for incomplete melting (heating) and subsequent solidification (cooling). Numbers indicate the sequence, arrows the direction of temperature changes.

The model is switched and the process is restarted by setting $T_0 = T_f$ and $\xi_0 = \xi_f$.

5. Simulation studies at material level

5.1. Prediction of liquid mass phase fractions

The hysteresis models consider temperature T as an input and predict the resulting change in the phase fraction $\xi(T)$. In Figures 7 and 8 phase transitions are induced by (drifting) sinusoidal temperature variations over time. It is noted that, due to rate-independence of the presented hysteresis models, a change in temperature directly induces a change in the phase fraction value without a time delay. Thus, changes in the frequency of the sinusoidal temperature profile do not change the predicted phase fraction values: the computed (T, ξ)-pairs are the same, see Barz and Sommer (2018) for a discussion on that point.

Figure 7 shows results for Rubitherm RT64HC. The hysteresis models are parametrized using the identified phase transition functions shown in Figure 1 (right). In addition $T^{\min}$ and $T^{\max}$ are set to 58°C and 65.5°C, respectively. These values are needed for the 'curve track' and 'curve switch' model. For each model, the triggered events which initiate a model switch are marked by circles or stars.

The phase fraction evolutions $\xi(t)$ are shown for each model in the respective subfigures on the left above. It can be seen that for the 'curve track' model between $t = 200$ and 300 the phase transitions are almost complete during increasing/decreasing temperatures. In contrast, for the 'curve switch' and 'curve scale' models between $t = 200$ and 300 the phase transitions are incomplete (ξ does not reach 0). Moreover, in the (T, ξ)-plane (shown on the right in Figure 7) it can be seen that the 'curve track' model almost exclusively uses the transition function for heating $\xi^{\mathrm{s}\to\mathrm{l}}$. This is confirmed by the corresponding figures on the left side: the event $T = T^{\max}$ which initiates the model switch to the transition function for cooling $\xi^{\mathrm{l}\to\mathrm{s}}$ occurs late at $t = 307$.

Finally, the 'curve switch' model predicts *non-smooth* phase fraction evolutions $\xi(t)$ during *smooth* monotonous (increasing

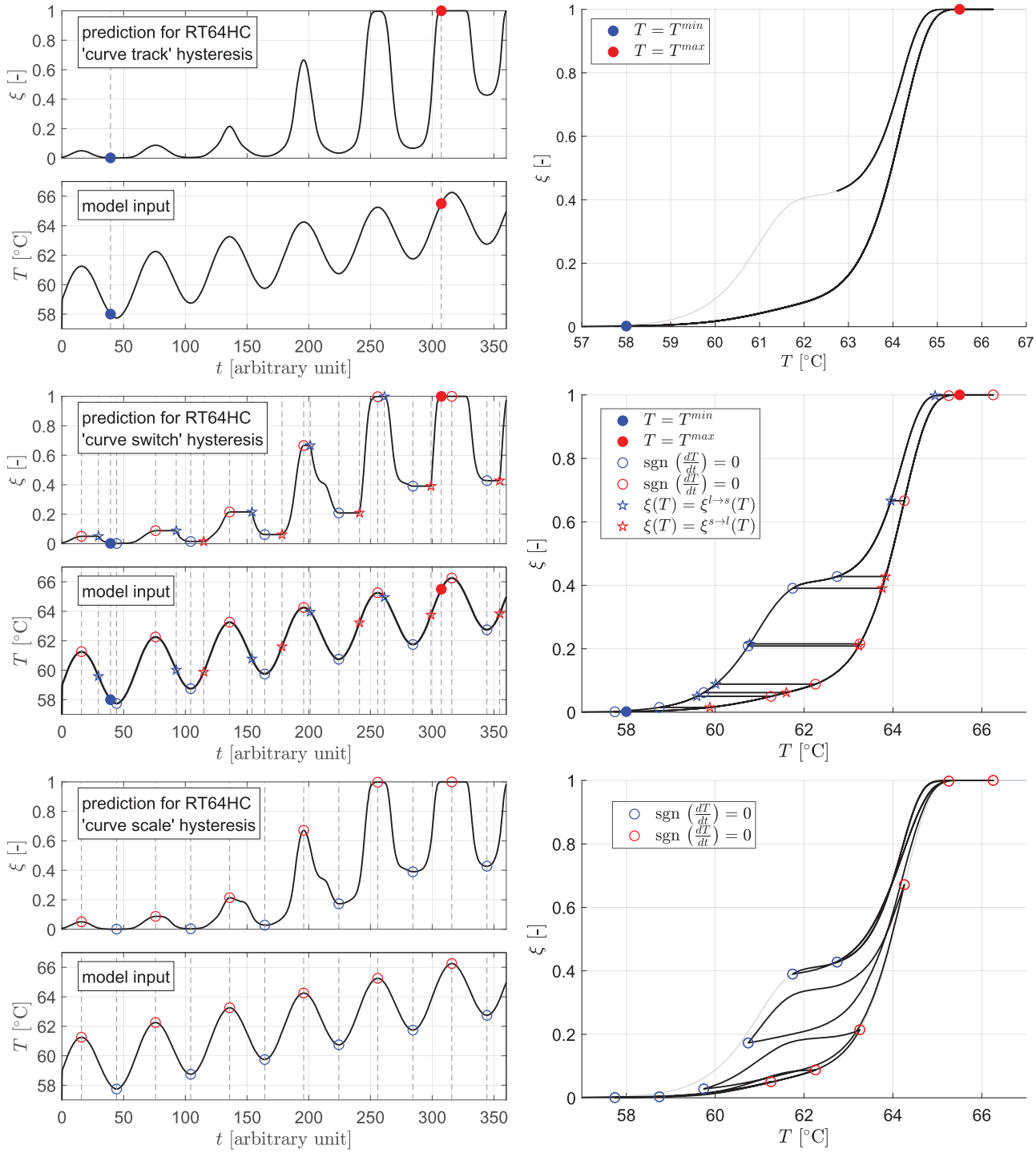

Figure 7. Predicted temperature-induced phase transitions for 'curve track' (Figures 1–3 above), 'curve switch' (Figures 4–6 middle), and 'curve scale' (Figures 7–9 below) hysteresis model using identified phase transition functions for Rubitherm RT64HC. Each subfigure applies the same sinusoidal temperature profile: Left below: temperature input to the model. Left above: predicted phase fraction evolution. Right: predictions in the (T, ξ)-plane. Note that time is given in arbitrary units, as the results are independent from the rate of temperature variations.

or decreasing) changes in $T(t)$. Corresponding sudden changes in the gradient of $\xi(t)$ occur when the events $\xi(T) = \xi^{s\to l}(T)$ or $\xi(T) = \xi^{l\to s}(T)$ in (13c) are triggered. The occurrence is marked by a star in Figure 7. These events indicate that a 'curve switch' is completed. In other words, the transition model switches from the connecting line model in Equation (12c) (with constant $\xi(T)$) to either of the complete transition models in Equations (12a) and (12b). Despite this, it is noted that all models produce smooth responses in $\xi(T)$ for smooth direction changes in $T(t)$.

Figure 8 shows results for Rubitherm SP50, where the hysteresis models are parametrized using the identified phase transition functions shown in Figure 2 (right) and with $T^{\min} = 40°C$ and $T^{\max} = 54°C$. The behaviour for the different models are qualitatively the same as in Figure 7. However, the differences between

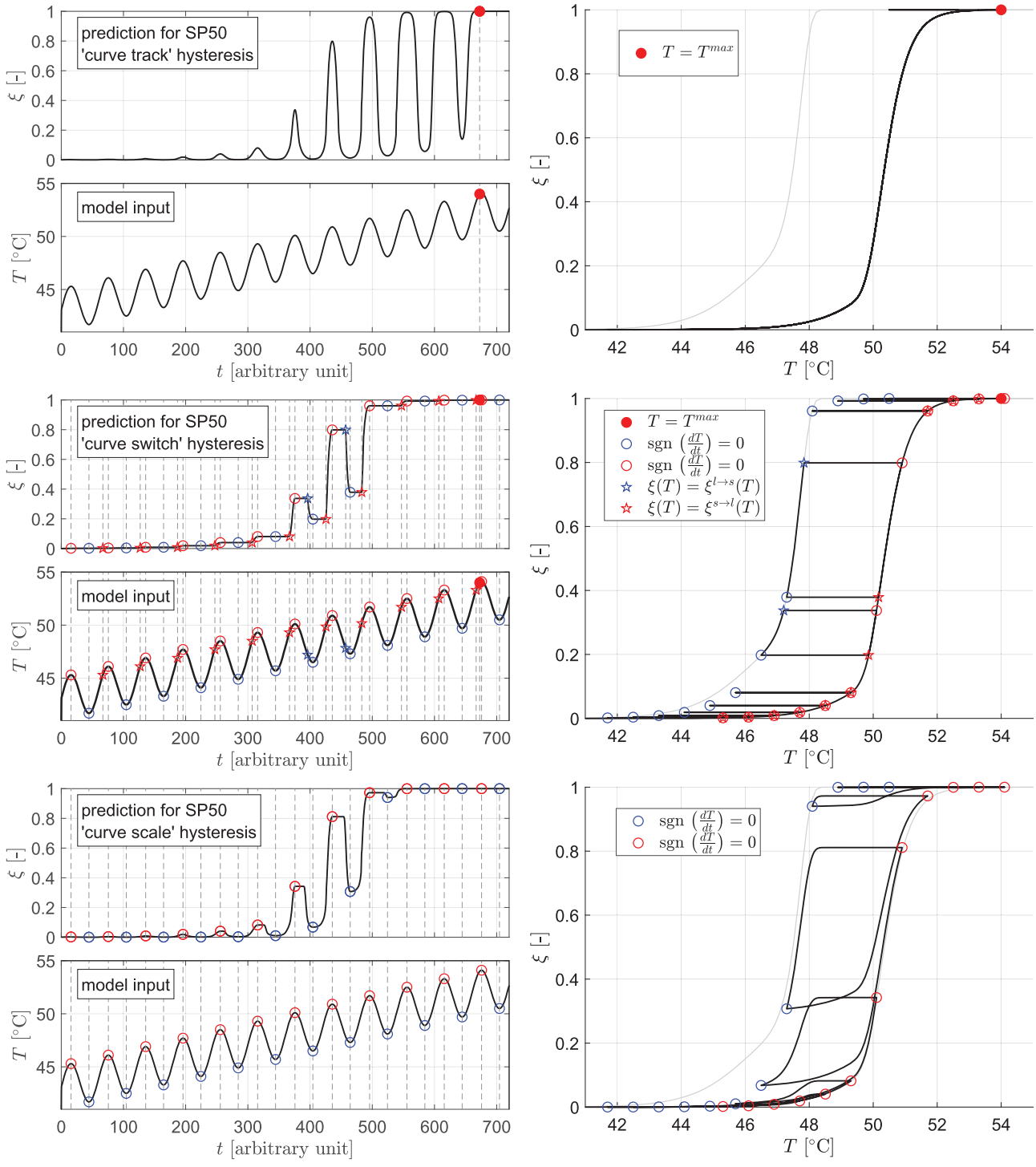

Figure 8. Predicted temperature-induced phase transitions for 'curve track' (Figures 1–3 above), 'curve switch' (Figures 4–6 middle), and 'curve scale' (Figures 7–9 below) hysteresis model using identified phase transition functions for Rubitherm SP50. Each subfigure applies the same sinusoidal temperature profile: Left below: temperature input to the model. Left above: predicted phase fraction evolution. Right: predictions in the (T, ξ)-plane. Note that time is given in arbitrary units, as the results are independent from the rate of temperature variations.

the 'curve track' model and the two other models are more pronounced, compare $\xi(t)$ between $t = 300$ and 700.

5.2. Prediction of enthalpy–temperature curves

It is studied how the selection of the different hysteresis models in Section 4 affects the prediction of PCM enthalpy–temperature curves during partial cyclic melting and solidification. These curves are relevant for the assessment of partial load operating conditions of LHTES. For doing so, PCM enthalpies are calculated by solving the hysteresis models together with Equation (7) for a given T_{ref}, with $T_{\text{ref}} < T^{\min}$.

Figures 9 and 10 show results from the temperature induced phase transition in the (T, h)-plane for Rubitherm SP50 and RT64HC, respectively. Starting from PCM solid state the temperature is increased and then oscillates (is alternately

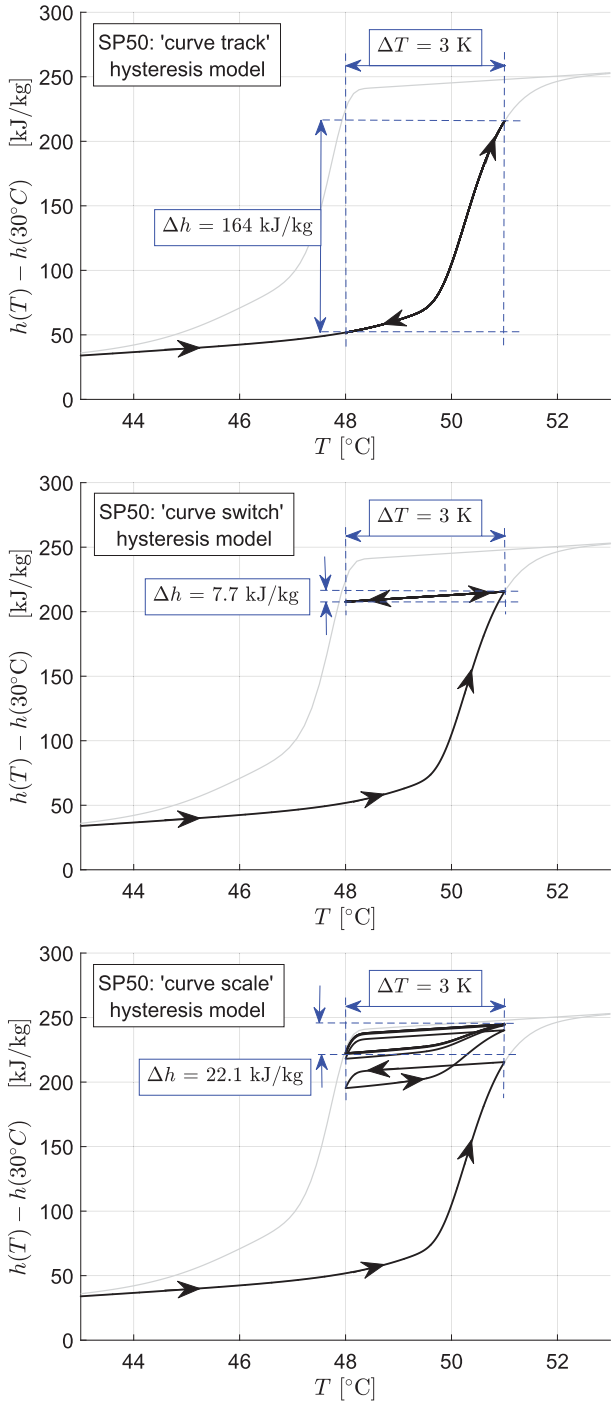

Figure 9. Predicted enthalpy–temperature curves in the (T, h)-plane for cyclic operation. PCM temperature is first increased from 30°C to 51°C and then alternately increased/decreased between 48°C and 51°C. Results from 'curve track' (first), 'curve switch' (second), and 'curve scale' (third) hysteresis model using identified phase transition functions for Rubitherm SP50.

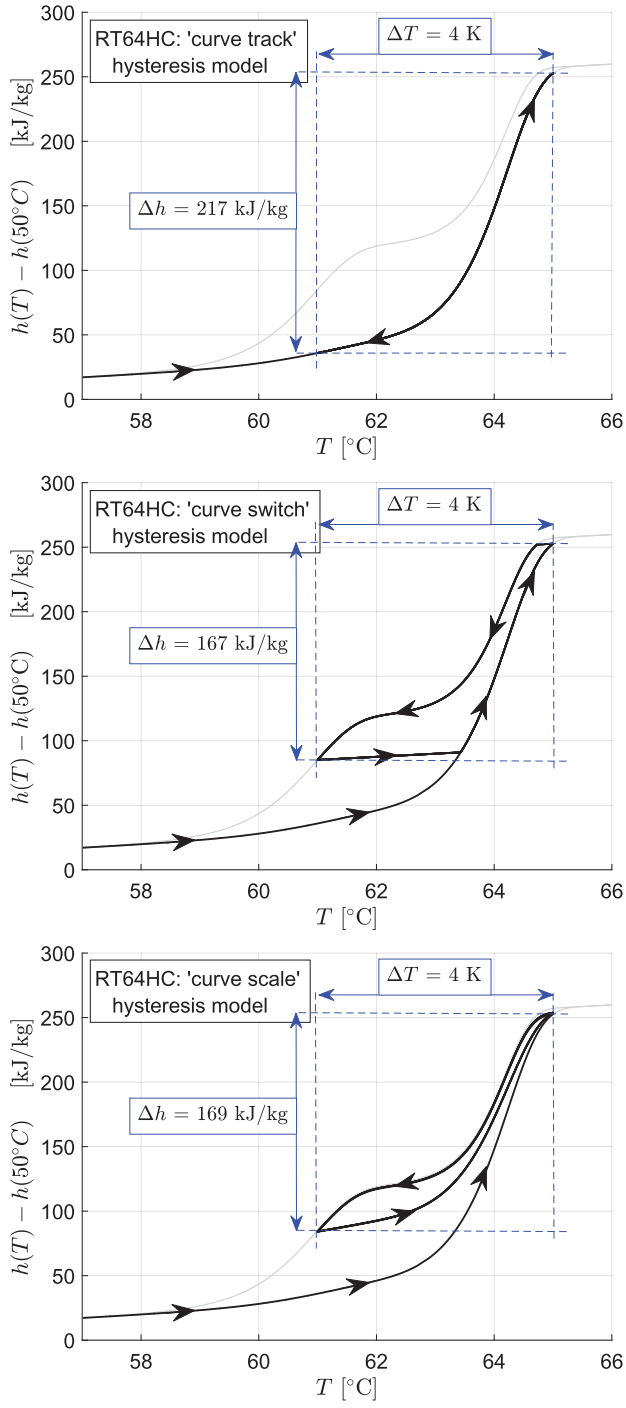

Figure 10. Predicted enthalpy–temperature curves in the (T, h)-plane for cyclic operation. PCM temperature is first increased from 50°C to 65°C and then alternately increased/decreased between 61°C and 65°C. Results from 'curve track' (first), 'curve switch' (second), and 'curve scale' (third) hysteresis model using identified phase transition functions for Rubitherm RT64HC.

increased/decreased) between a minimum and maximum temperature within the phase transition temperature range.

For both PCM materials it can be clearly seen that the predicted amount of absorbed/released heat is very different for the different models. The biggest difference exists for the 'curve track' model. This is to be expected, as this model does not account for hysteresis phenomena during incomplete transitions. However, the 'curve switch' and 'curve scale' model also show very different results, especially when the induced temperature variations are too small to finish the curve switch in the 'curve switch' model. This is shown in Figure 9 in the second subfigure where the temperature decrease during the cycles is not sufficient to reach the enthalpy–temperature curve for complete solidification $\xi^{\mathrm{l}\to\mathrm{s}}$. Thus, the phase fraction remains constant during the cycles and the predicted absorbed/released heat (7.7 kJ/kg) results from contributions of c_p^s and c_p^l only, see Equation (6).

6. Model validation at component level

The accuracy of the different phase transition hysteresis models is assessed by comparing experimental data with model predictions for a LHTES shown in Figure 11. The storage design corresponds to the so called compact heat exchanger design which is widely applied for air conditioning, refrigeration and in automotive and aerospace industry (Shah and Sekulic 2003). Specifically, it is an aluminium plate-fin extended surfaces heat exchanger with 19 parallel liquid passages of 3 mm height, and 20 air passages of 10 mm height. Liquid and air passage use offset strip fins (width 0.3 mm) of rectangular cross section with 1.95 and 2.4 mm rib separation, respectively. Water is used as heat transfer fluid. The air passages are filled with 11.4 litres PCM RT64HC.

The water flow rate through the storage is measured at the inlet by electromagnetic flow sensor SIEMENS SITRANS F M MAG 3100. According to the calibration certificate, the measurement errors range between ± 0.07 and 0.15% for a flow range of 30–145 L/min. The water in- and outlet storage temperatures and the PCM temperature are measured by class A/0°C, 3-wire PT 100 Ohm temperature sensors with a measurement error of $\pm 0.15 - 0.35$ K in a temperature range of 0–100°C. PCM temperature sensors are installed in one PCM passage at three positions, two close to the PCM passage wall and one in the middle of the PCM passage (see also Figure 11 right).

6.1. Numerical modelling of the LHTES

The LHTES is a dynamic distributed parameter system with internal temperature fields. The LHTES model consists of dynamic energy balance equations for: the water passing the collector/distributor at the storage in- and outlet (1D in water flow direction); the thermal mass of the aluminium storage container and collector (lumped model); the water forced convective flow through the water passages (1D in axial water flow direction) neglecting heat conduction; the thermal mass of the passage wall with corresponding fins of the water and PCM side (1D in axial water flow direction); and the PCM in the PCM passages (1D perpendicular to the axial water flow direction) neglecting the heat conduction in axial direction. The outer storage wall is endowed with a thermal insulation, heat losses to the surroundings are neglected.

For each water passage the same inflow and outflow conditions are assumed. In addition, it is assumed that all water passages and PCM passages are equal and no heat is exchanged between adjacent water passages. Based on these assumptions, only one water passage with a surrounding PCM needs to be considered for the modelling. To this end, an average fluid flow and effective boundary conditions are used. The heat transfer between water and water passage walls is calculated using correlations for plate-fin extended surfaces geometries with offset strip fins by Manglik and Bergles (1995), Rohsenow, Hartnett, and Cho (1998, 17.85). The total extended heat transfer area in all 19 microchannels of the water passages is 5 m^2. All experiments are conducted at a constant water volumetric flow of 90 L/h. This results in low water flow velocities of 4.4 mm/s inside each water passage with Reynolds numbers equal to 22. Despite these relatively low Reynolds numbers the calculated convective heat transfer between water and extended surface microchannels is high with 1144 $W/m^2/K$.

The mathematical modelling of the conductive heat transfer in the 1D PCM modelling domain employs the so-called weak formulation approach, in which the governing heat equation reads as a single-phase equation without explicitly treating the moving solid/liquid interface (Voller, Swaminathan, and Thomas 1990; Hu and Argyropoulos 1996). A mushy transition zone between the two phases is considered, and the effective specific heat capacity in Equation (6) is used to model heat

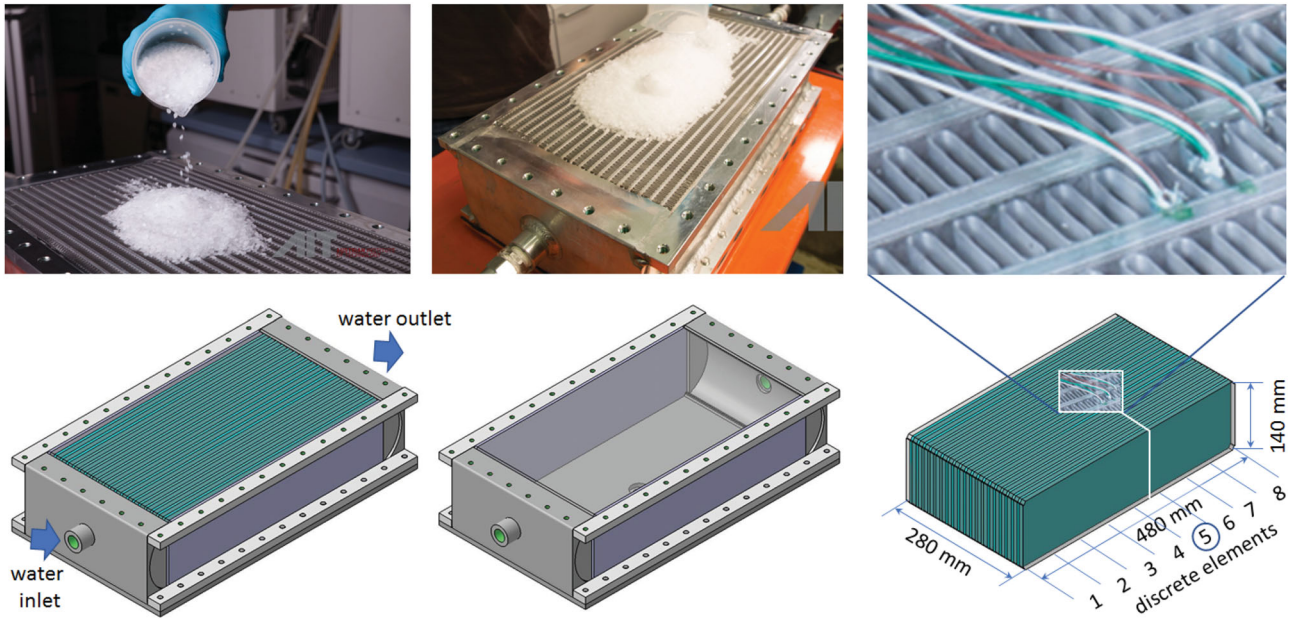

Figure 11. Compact air/liquid plate fin heat exchanger. The air passages are filled with PCM (PCM side). Water flows through the liquid passages (water side). Three temperature sensors are installed to measure temperatures inside one PCM passage (they are located at the fifth discrete element in water flow direction of the numerical LHTES model).

transfer with phase change. As discussed in Section 2.2, mixed PCM properties are defined as functions of the phase fraction.

Fixed grid spatial discretization is applied to all 1D dynamic energy balance equations: first-order upwind schemes are used for the convective heat transfer in the water, and central difference scheme is applied for the conduction heat transfer in the passage wall and in the PCM. In axial water flow direction along the passages eight elements were used (see Figure 11), for the PCM two elements were used perpendicular to the axial direction. Thus, temperature fields inside the PCM are approximated by 16 elements. For each element an ordinary differential equation (ODE) is derived whose solution yields the corresponding PCM temperature. The PCM effective properties $\tilde{c}$, $\tilde{\rho}$ and $\tilde{\lambda}$ of each element are evaluated using the property relations in Section 2.2 together with the phase transition hysteresis models in Section 4. During the solution of the 16 ODEs model switching conditions are monitored and corresponding events are triggered, i.e. if a condition is fulfilled the integration is terminated and the model is switched. It is noted that all switching conditions are implicitly defined, i.e. their occurrence in time is state-dependent and therefore their exact localization requires a continuous monitoring of corresponding states during the solution of the ODEs.

6.2. Identification of phase transition functions and PCM effective properties

In Section 3, RT64HC heat capacities c_p^s, c_p^l and Δh_t as well as the phase transition functions for heating $\xi^{s\to l}$ and cooling $\xi^{l\to s}$ were identified from heat capacity data (taken from the PCM manufacturer's data sheet). However, it was found that predictions with the numerical LHTES model can be improved when using PCM heat capacities and transition functions identified by fitting PCM temperature measurements taken from the LHTES.

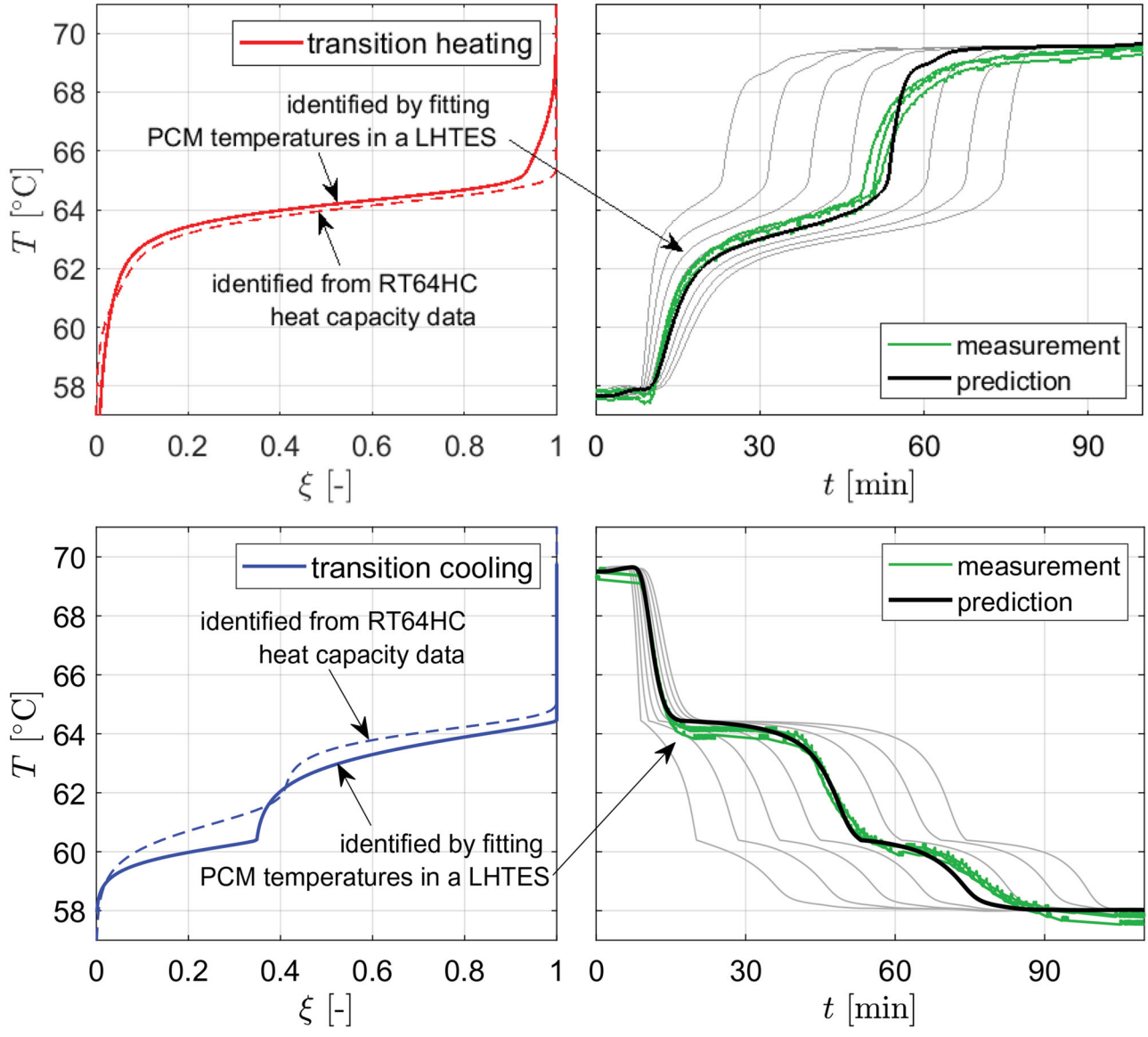

Figure 12. Identification of phase transition functions for heating $\xi^{s\to l}$ and cooling $\xi^{l\to s}$ for Rubitherm RT64HC. Left: predicted phase transitions in the (ξ, T)-plane (axes are flipped); Right: measured (dotted green) and predicted (solid black) PCM temperatures at the fifth discrete element in flow direction as indicated in Figure 11. Solid grey lines show predictions at all other discrete elements 1, 2, 3, 4, 6, 7, 8. Transition functions depicted by solid lines (on the left) show the results for fitting PCM temperatures (on the right) in a LHTES during complete melting (above) and complete solidification (below). Dashed lines show the results from fitting RT64HC heat capacity data (taken from Figure 1 right). Model predictions are calculated using the LHTES model in Section 6.1.

Table 1. Numerical performance and quality of predictions (fitting) for the LHTES. Experiment designs indicated by: H – complete transition for (H)eating; C – complete transition for (C)ooling; h – incomplete transition for (h)eating; c – incomplete transition for (c)ooling. All computations have been carried out in MATLAB on an Intel® Core™ 2 Duo Processor E6600 @2.40-GHz computer with 4 GB RAM. The ODEs (initial value problems) have been solved using MATLAB ode15s solver with relative and absolute error tolerance equal 1E−7.

Experiment		Model	Simulation		Fitting	
					Absolute error	
Number (ref.)	Design	Curve	Computation time	Number of restarts	Mean	Max
Experiments for identification						
1 (Figure 12(a))	H	–	17 s	–	0.29 K	1.1 K
2 (Figure 12(b))	C	–	24 s	–	0.20 K	0.6 K
Cross-validation experiments for assessment of predictive performance						
3 (Figure 13)	c,h,c,h,c,H	Track	118 s	46	0.73 K	4.2 K
		Switch	169 s	295	0.42 K	3.5 K
		Scale	196 s	194	0.31 K	2.0 K
4	c,h,c,H,C,H	Track	138 s	62	0.56 K	4.2 K
		Switch	167 s	260	0.37 K	4.2 K
		Scale	206 s	166	0.29 K	1.3 K
5	c,h,c,h,C	Track	69 s	30	0.87 K	2.7 K
		Switch	88 s	134	0.54 K	2.4 K
		Scale	105 s	68	0.41 K	1.8 K
6 (Figure 14)	h,c,h,c,H	Track	43 s	24	0.57 K	3.6 K
		Switch	139 s	291	0.52 K	3.3 K
		Scale	163 s	213	0.42 K	3.5 K
7	h,c,h,c,h,C	Track	31 s	32	0.52 K	2.6 K
		Switch	100 s	199	0.84 K	2.7 K
		Scale	116 s	132	0.51 K	2.0 K
8	h,c,h,c,h,C	Track	38 s	24	0.75 K	3.0 K
		Switch	101 s	203	0.75 K	2.4 K
		Scale	175 s	126	0.59 K	2.0 K

Accordingly, a non-linear regression problem was solved using the LHTES model in Section 6.1. Predicted PCM temperatures at the fifth discrete element in axial flow direction (indicated in Figure 11) in the middle of the PCM passage were fitted to recorded PCM temperatures. This was done for one heating experiment and one cooling experiment. Results are shown in Figure 12. In addition, mean and maximum values of the absolute fitting errors are given in Table 1, where the heating experiment corresponds to experiment number 1 and the cooling experiment to experiment number 2. It is noted that the measured PCM temperatures at the three positions (indicated in Figure 11) do not differ much from each other. This indicates that heat transfer is not critically controlled by heat conduction inside the PCM. The main reasons are the relatively dense fin arrangement, the small height of the PCM passages and the relatively low volumetric water flow rates of the conducted experiments.

For $\xi^{s\to l}$, a superposition of two Gumbel Minimum distribution functions ϕ_1^G and ϕ_2^G were fitted (see Equation (3) and (5)), with: $\mu_1 = 338.1$, $\beta_1 = 2.5$, $\kappa_1 = 1$, $w_1 = 0.2$, and $\mu_2 = 337.5$, $\beta_2 = 0.5$, $\kappa_2 = 1$, $w_2 = 0.8$. For $\xi^{l\to s}$, a superposition of two adapted Weibull distribution functions ϕ_1^W and ϕ_2^W were fitted (see Equation (4) and (5)), with: $\mu_1 = 333.54, \alpha_1 = 0.65, \gamma_1 = 1.3$, $w_1 = 0.34$, and $\mu_2 = 337.59$, $\alpha_2 = 1.2$, $\gamma_2 = 1.3$, $w_2 = 0.66$. The estimated heat capacity and phase transition enthalpy values (same for heating and for cooling) are: $c_p^s = c_p^l = 2.7\,\mathrm{kJ/kg/K}$ and $\Delta h_t = 240.8\,\mathrm{kJ/kg}$. In addition, values for the parameters of the 'curve track' and the 'curve switch' model $T^{\min} = 58.5$ and $T^{\max} = 67.5$ were defined. Effective density $\tilde{\rho}$ and thermal conductivity $\tilde{\lambda}$ in Equation (8) are calculated using the data given by Rubitherm: $\rho^s = 880.0$, $\rho^l = 780.0$, and $\lambda^s = \lambda^l = 0.2$, respectively. The estimated values for c_p^s, c_p^l and Δh_t are greater (13% and 9%) than the estimated values using heat capacity data from Rubitherm in Figure 1. Deviations in the estimated transition functions are shown in Figure 12.

In the same way as in Section 3.1, the quality of the parameter estimates is assessed by an identifiability analysis. For heating, the analysis diagnoses a rank-deficient problem. The condition number of the sensitivity matrix is 2353, the singular values are between 5.0 and 11,754, and the collinearity index is 0.20. For cooling, the problem is also rank-deficient. The condition number is 1618, the singular values are between 7.4 and 11,902, and the collinearity index is 0.14. In conclusion, for heating and cooling, all estimated parameter values are not severely affected by the ill-conditioning of the sensitivity matrix.

For heating five out of seven parameters can be reliably estimated. For cooling seven out of nine parameters can be reliably estimated. The ranking of parameters regarding their linear independence and sensitivity yields the following decreasing order for heating: μ_2, μ_1, Δh_t, β_2, w_1, β_1, c_p, and for cooling: μ_2, μ_1, Δh_t, w_1, α_2, α_1, γ_2, γ_1, c_p. The same conclusion as in Section 3.1 can be drawn, the location parameters of the distribution functions μ_i and the phase transition enthalpy Δh_T can be most reliably estimated. Compared with results from Section 3.1, the total number of parameters which can be reliably estimated is significantly increased. This is most likely because in this section the regression problems are defined using a dense sampling of PCM temperature profiles, while in Section 3.1, the available heat capacity data is sparse. It can be concluded that the recorded PCM temperature profiles give a good representation of the phase transition behaviour. They can be used for the identification of shape parameters of the selected transition functions.

6.3. Predictive performance

Besides the experiments performed for the identification of the transition functions for heating and cooling (see Table 1 experiments 1 and 2), six additional experiments (see Table 1 experiments 3–8) were performed for the validation of the different hysteresis models. These experiments realize alternating heating and cooling operation with incomplete phase transitions (incomplete melting and solidification). Table 1 gives an overview about the experiment designs of each individual experiment. It is noted that the validation of the predictive performance is carried out using the identified parameters from experiments 1 and 2. Experiments 3–8 have been used for validation only (not for identification). Thus, the predictive performance of the different hysteresis models is assessed by cross-validation.

In the same way as for the identification experiments 1 and 2, the cross-validation experiments 3–8 are evaluated based on the fitting of recorded PCM temperatures. Corresponding predictions of the numerical LHTES model were taken from the middle of the PCM passage at the fifth discrete element in axial flow direction (see Figure 11). Results from experiments 3 and 4 are shown in Figures 13 and 14, respectively. In Figure 13 the shortcomings of the 'curve track' model can be clearly seen. The model uses the cooling curve only for predicting phase fractions and temperatures during incomplete phase transitions in the temperature range between 60°C and 64°C in the

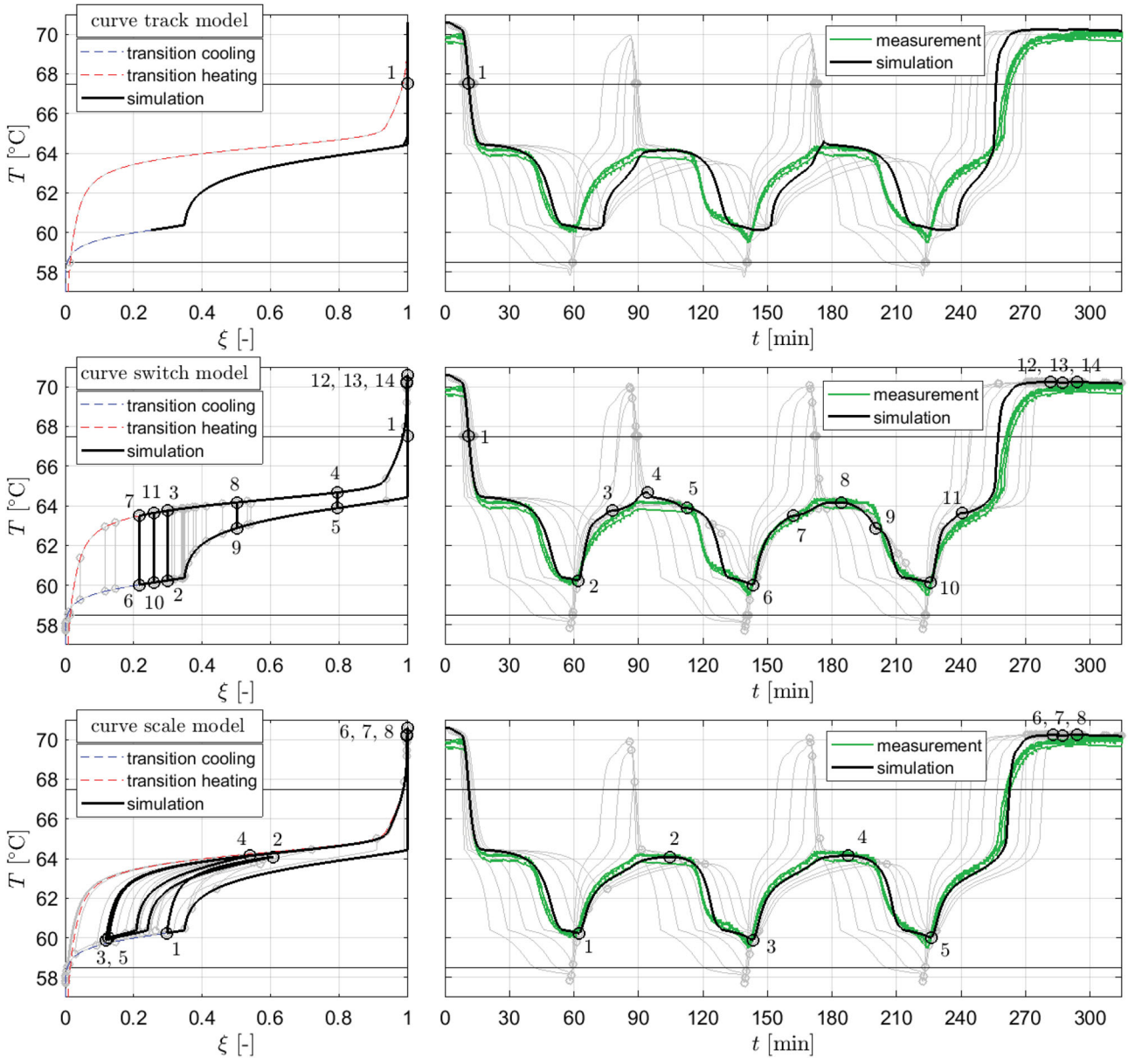

Figure 13. Comparison of predicted and measured PCM temperatures during partial melting and solidification using the LHTES model in Section 6.1 together with the following phase transition hysteresis models, above: 'curve track'; middle: 'curve switch'; below: 'curve scale' hysteresis model. The same phase transition functions for heating $\xi^{s\to l}$ and cooling $\xi^{l\to s}$ in Figure 12 left were used for the parametrization of all three hysteresis models. Left: predicted phase transitions in the (ξ, T)-plane (axes are flipped); Right: measured (dotted green) and predicted (solid black) PCM temperatures at the fifth discrete element in flow direction as indicated in Figure 11. Solid grey lines show predictions at all other discrete elements 1, 2, 3, 4, 6, 7, 8. Occurrences of events and corresponding restarts of the simulation are indicated by circles. The numbers highlight the sequence of restarts for predicted PCM temperatures at the measurement position.

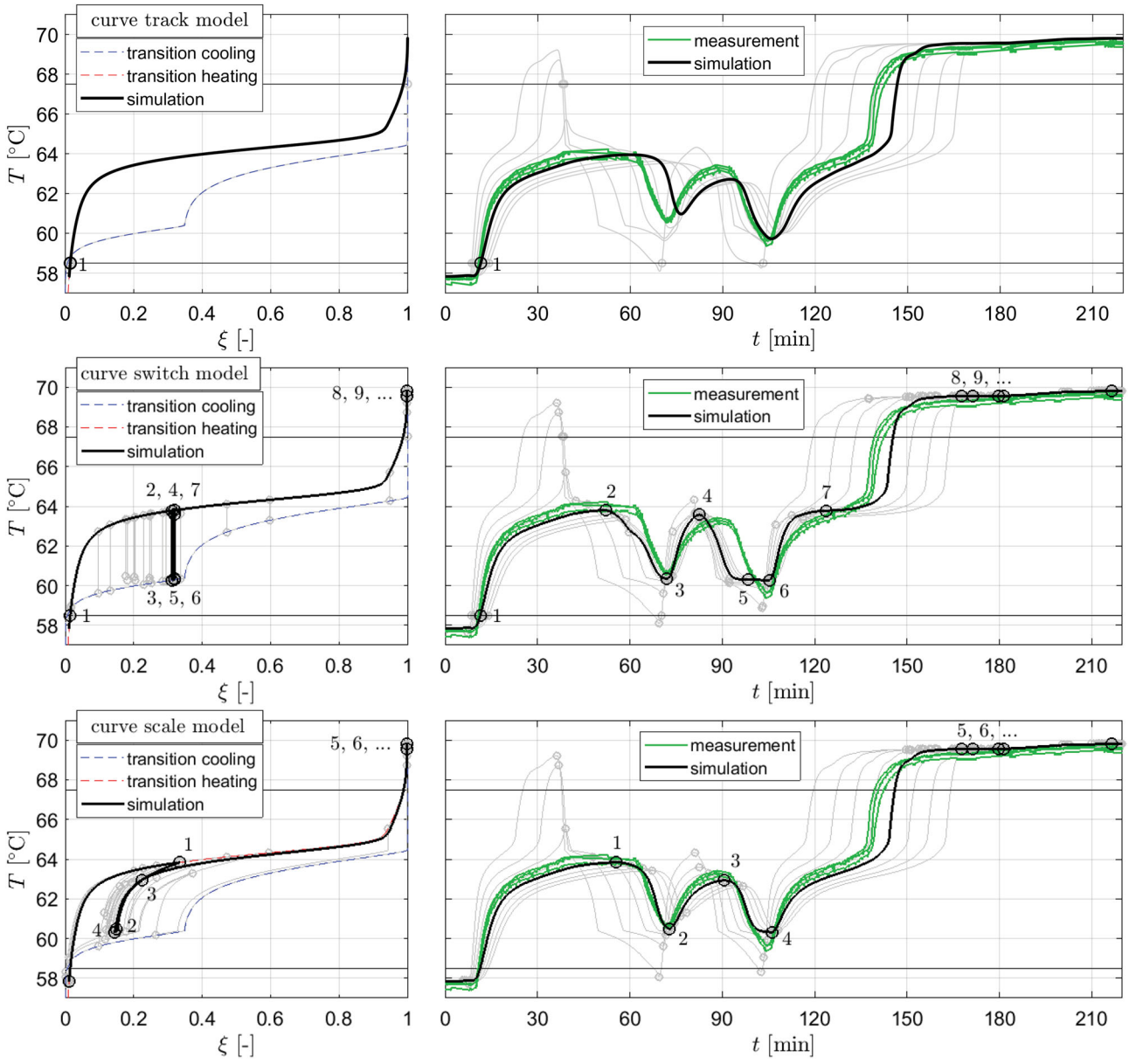

Figure 14. Comparison of predicted and measured PCM temperatures during partial melting and solidification using the LHTES model in Section 6.1 together with the following phase transition hysteresis models, above: 'curve track'; middle: 'curve switch'; below: 'curve scale' hysteresis model. The same phase transition functions for heating $\xi^{s\to l}$ and cooling $\xi^{l\to s}$ in Figure 12 left were used for the parametrization of all three hysteresis models. Left: predicted phase transitions in the (ξ, T)-plane (axes are flipped); Right: measured (dotted green) and predicted (solid black) PCM temperatures at the fifth discrete element in flow direction as indicated in Figure 11. Solid grey lines show predictions at all other discrete elements 1, 2, 3, 4, 6, 7, 8. Occurrences of events and corresponding restarts of the simulation are indicated by circles. The numbers highlight the sequence of restarts for predicted PCM temperatures at the measurement position.

time window from 60 to 260 min. Qualitative much better fitting is obtained for the 'curve switch' model which implements switches between heating and cooling curves for alternating heating and cooling inside the phase transition temperature range. Finally, the 'curve scale' model shows even better results implementing the scaling the heating and cooling curves for alternating heating and cooling.

Figure 14 shows the same results in terms of the comparatively poor predicitive performance of the 'curve track' model. Here the heating curve only is used to predict phase fractions and temperatures for alternating heating and cooling operation with incomplete phase transitions. Compared with experiment 3 in Figure 13, the heating and cooling operation in experiment 4 in Figure 14 realizes phase transitions in a smaller temperature range with PCM temperatures $> 60°C$ and $< 64°C$ in the time window from 50 to 120 min. It can be seen that for this time window the 'curve switch' model implements the curve switch using a connecting line between heating and cooling curve and a constant ξ. For this constant ξ and the realized minimum and maximum PCM temperatures the heating and cooling curves are never reached and the 'curve switch' model implements the constant ξ for the whole time window. The corresponding predictions are of poor quality indicating shortcomings of the 'curve switch' model for this operating mode. In contrast, the 'curve scale' model gives much better results implementing the scaling of heating and cooling curves.

Table 1 shows the mean and absolute fitting errors for all experiments. These quantitative results clearly support the findings above. In four out of six experiments the 'curve track' model shows the poorest performance in terms of the mean absolute fitting error. For the remaining two experiments the 'curve switch' model gives equal or higher errors. The 'curve scale' model always gives best results with the lowest mean absolute fitting errors for all experiments. Compared with the maximum error values found for each experiment, the average error reduction by the 'curve scale' model is around 53% (ranging from 27% to 92%).

The maximum absolute errors for each experiment show the same trend. In four out of six experiments the 'curve track' model shows the poorest performance. For the remaining two experiments the 'curve switch' model gives equal or higher maximum absolute errors. Except for experiment 6, the 'curve scale' model gives always best results in terms of the maximum absolute errors. Compared with the maximum error values found for each experiment, the average error reduction by the 'curve scale' model is around 43% (ranging from 7% to 70%).

6.4. Numerical performance

Table 1 lists quantitative results for the numerical performance of the different phase transition models linked to the LHTES energy balance equation model.

All hysteresis models are discontinuous, with implicit (state-dependent) switches, see Sections 4.1–4.3. During integration (simulation) the switching events are detected, models are switched and integration is restarted. These model switches and corresponding restarts occur for experiments 3–8 with partial load conditions and incomplete phase transitions. For experiment 3 in Figure 13 and experiment 6 in Figure 14 the occurrence of detected events and corresponding model switches are marekd by circles. In addition, for the PCM temperatures at the measurement position numbers are used to indicate the sequence. The total number of restarts for each experiment is given in Table 1. Generally, the calculation times for model integration increase with the number of switches triggered during a simulation. Accordingly, the 'curve track' model with the lowest number of restarts for each experiment also needs the shortest calculation times. However, comparing the numbers for the 'curve switch' with the 'curve scale' model, it can be seen that although the highest number of restarts are always found for the 'curve switch' model, the 'curve scale' model needs the longest calculation times. This can be explained by a higher non-linearity of the 'curve scale' model when compared with the 'curve switch' model. The latter uses a constant ξ during the curve switch. This means constant PCM properties are implemented, see Equations (6)–(8). In contrast, the 'curve scale' model always implements non-linear PCM properties during phase transition which increases the model complexity and thus, yields higher calculation times.

It is noted that the given computation times are achieved with a straightforward implementation using MATLAB integrator ODE15s with the build-in event location function. Here the integration is terminated if an event is detected. After switching the model the integrator has to be restarted. These starting phases turn out to be time consuming (Brand-Pollmann 2004). State-of-the-art integrators with an appropriate event detection (Brand-Pollmann 2004; Bock et al. 2018) do not require a complete restart of the integration process and therefore can significantly decrease calculation times.

7. Discussion and conclusions

This contribution discusses the application of three different hysteresis models for the prediction of temperature-induced phase transitions in solid/liquid PCM. These models are the 'curve track', 'curve switch' and the 'curve scale' models. The first two models have already been implemented in commercial building simulation and/or multiphysics software. For the third model proposed in this contribution no such implementation exists. All models consider a hysteresis in phase fraction originating from positive (heating) and negative (cooling) temperature rates and the temperature history.

The presented phase transition models are phenomenological models. They are directly identified using data for complete melting and solidification experiments only. This means a reduced effort for model calibration, e.g. available heat capacity data as provided by PCM manufacturers can be used. However, it should also be noted that the PCM phase transition behaviour, i.e. the characteristic temperatures, such as temperature hysteresis/supercooling and phase change onset temperatures, and phase transition enthalpies are each individual functions of the heating/cooling rates used in calorimetric measurements. Specific measurement protocols exist for an accurate determination of each quantity, e.g. Desgrosseilliers et al. (2013); Vidi et al. (2015). Accordingly, using data from a single measurement protocol (in this contribution the data from the PCM manufacturer) for identification of phase transition models, might limit the accuracy of model predictions.

Compared with other works which model the phase transition behaviour by enthalpy–temperature curves, this contribution proposes using (liquid mass) phase fraction–temperature curves. In doing so, within the phase transition temperature range, one phase transition model can be used to predict all, so called 'effective' thermo-physical PCM properties. This means, e.g. effective specific heat capacity, effective enthalpy and effective density are modelled by a superposition of corresponding solid and liquid PCM properties using the phase fraction as a weighting factor.

While the 'curve track' model accounts for hysteresis effects for complete melting and solidification only, the 'curve switch' and the 'curve scale' models also account for hysteresis within the phase transition temperature range, i.e. for incomplete phase transitions. This is especially relevant for the characterization of LHTES operating under partial load conditions. Simulation studies are presented for Rubitherm's PCM RT64HC (a paraffin) and SP50 (a salt water mixture with additives). The results highlight significant differences between each model in the predicted absorbed and released energies for cyclic incomplete melting and solidification. The experimental validation is performed linking the three models with a numerical energy balance equation model of a LHTES filled with RT64HC. Six cross-validation experiments were considered with in total 26 partial load conditions and corresponding incomplete phase transitions. The quantitative analysis of recorded PCM temperatures

clearly indicate the best predictive performance of the 'curve scale' model, i.e. the novel modelling approach proposed in this contribution.

It is noted that dynamic computations with all presented hysteresis models have to be carried out with solvers with event detection (root finding) for handling the switching between submodels, e.g. between the phase transition functions for heating (solid-to-liquid transition function) and for cooling (liquid-to-solid transition function). In the 'curve scale' model events are triggered based on the monitoring of one condition only, namely $\mathrm{sgn}(\mathrm{d}T/\mathrm{d}t) = 0$. Thus, compared with the 'curve switch' model (the hysteresis model with the second-best predictive performance) it is easier to implement in a simulation software and it is likely to be the more robust numerical model. Using a straightforward MATLAB implementation, each model switch needs a complete restart of the numerical integration process. Corresponding starting phases turn out to be time consuming. This is especially relevant for numerical LHTES models with a spatial discretization on fine grids where each grid point is linked with one hysteresis model. The simulation studies with the LHTES model in this contribution show the longest calculation times for the 'curve scale' model. If available, alternative integrators with an appropriate event detection are recommendable as they can significantly decrease calculation times.

Finally, it is noted that all presented models are static hysteresis models. They are rate-independent in the sense, that, e.g. increased heating rates lead to faster melting but result in the same phase fraction value for any stopping temperature. Accordingly, also the magnitude of the hysteresis is rate-independent. This simplification certainly limits the predictive performance of all presented hysteresis models. Another important issue is that the studied hysteresis phenomena are usually scale dependent, as discussed e.g. in Noël et al. (2016). It is thus recommendable to parametrize the hysteresis models using data generated at temperature rates and scales that match the heating and cooling rates and system size of the intended application. For example, as discussed in this contribution, the hysteresis models might be directly parametrized using data from storage internal PCM temperature measurements recorded during complete charging and discharging operation.

Note

1. It is noted that, from a thermodynamic view-point, the models are not state functions. This is because the predicted states are path-dependent as they depend on the direction of applied temperature rates.

Acknowledgements

The authors thank Birgo Nitsch, Vladimir Parfenov and Andreas Strehlow (AKG Verwaltungsgesellschaft mbH) for fruitful discussion and support in the modelling of the heat transfer in the compact plate fin heat exchanger. The authors would like to thank the Catalan Government for the quality accreditation given to their research group (GREiA 2017 SGR 1537). GREiA is certified agent TECNIO in the category of technology developers from the Government of Catalonia.

Disclosure statement

No potential conflict of interest was reported by the authors.

Funding

This project has received funding from the European Union's Horizon 2020 research and innovation programme [grant number 768824] (HYBUILD) and from the Ministerio de Economía y Competitividad de España (ENE2015-64117-C5-1-R (MINECO/FEDER)).

ORCID

Tilman Barz http://orcid.org/0000-0001-7289-3627

References

Al-Saadi, Saleh Nasser, and Zhiqiang John Zhai. 2013. "Modeling Phase Change Materials Embedded in Building Enclosure: A Review." *Renewable and Sustainable Energy Reviews* 21: 659–673.

Barz, Tilman, and Andreas Sommer. 2018. "Modeling Hysteresis in the Phase Transition of Industrial-Grade Solid/Liquid PCM for Thermal Energy Storages." *International Journal of Heat and Mass Transfer* 127: 701–713.

Biswas, Kaushik, Yash Shukla, Andre Desjarlais, and Rajan Rawal. 2018. "Thermal Characterization of Full-Scale PCM Products and Numerical Simulations, Including Hysteresis, to Evaluate Energy Impacts in an Envelope Application." *Applied Thermal Engineering* 138: 501–512.

Bock, H. G., C. Kirches, A. Meyer, and A. Potschka. 2018. "Numerical Solution of Optimal Control Problems with Explicit and Implicit Switches." *Optimization Methods and Software* 33 (3): 450–474.

Bony, J., and S. Citherlet. 2007. "Numerical Model and Experimental Validation of Heat Storage with Phase Change Materials." *Energy and Buildings* 39 (10): 1065–1072.

Brand-Pollmann, Ulrich. 2004. "Numerical Solution of Optimal Control Problems with Implicitly Defined Discontinuities with Applications in Engineering." PhD diss., Universität Heidelberg.

Delcroix, Benoit. 2015. "Modeling of Thermal Mass Energy Storage in Buildings with Phase Change Materials." PhD diss., École Polytechnique de Montréal, Montréal (QC, Canada).

Delcroix, Benoit, Michaël Kummert, and Ahmed Daoud. 2017. "Development and Numerical Validation of a New Model for Walls with Phase Change Materials Implemented in TRNSYS." *Journal of Building Performance Simulation* 10 (4): 422–437.

Desgrosseilliers, Louis, Catherine A. Whitman, Dominic Groulx, and Mary Anne White. 2013. "Dodecanoic Acid as a Promising Phase-Change Material for Thermal Energy Storage." *Applied Thermal Engineering* 53 (1): 37–41.

Diaconu, Bogdan M., and Mihai Cruceru. 2010. "Novel Concept of Composite Phase Change Material Wall System for Year-Round Thermal Energy Savings." *Energy and Buildings* 42 (10): 1759–1772.

Diaconu, B. M., S. Varga, and A. C. Oliveira. 2010. "Experimental Assessment of Heat Storage Properties and Heat Transfer Characteristics of a Phase Change Material Slurry for Air Conditioning Applications." *Applied Energy* 87 (2): 620–628.

Frei, Walter. 2016. "Thermal Modeling of Phase-Change Materials with Hysteresis." Accessed October 19, 2018. https://www.comsol.com/blogs/thermal-modeling-of-phase-change-materials-with-hysteresis/.

Gasia, Jaume, Alvaro deGracia, Gerard Peiró, Simone Arena, Giorgio Cau, and Luisa F. Cabeza. 2018. "Use of Partial Load Operating Conditions for Latent Thermal Energy Storage Management." *Applied Energy* 216 (C): 234–242.

Gaur, Umesh, and Bernhard Wunderlich. 1981. "Heat Capacity and Other Thermodynamic Properties of Linear Macromolecules. II. Polyethylene." *Journal of Physical and Chemical Reference Data* 10 (1): 119.

Goia, Francesco, Gaurav Chaudhary, and Stefano Fantucci. 2018. "Modeling and Experimental Validation of an Algorithm for Simulation of Hysteresis Effects in Phase Change Materials for Building Components." *Energy and Buildings* 174: 54–67.

Gowreesunker, B. L., and S. A. Tassou. 2013. "Effectiveness of CFD Simulation for the Performance Prediction of Phase Change Building Boards in the Thermal Environment Control of Indoor Spaces." *Building and Environment* 59: 612–625.

Gowreesunker, B. L., S. A. Tassou, and M. Kolokotroni. 2012. "Improved Simulation of Phase Change Processes in Applications Where Conduction is the Dominant Heat Transfer Mode." *Energy and Buildings* 47: 353–359.

Hu, H., and S. A. Argyropoulos. 1996. "Mathematical Modelling of Solidification and Melting: A Review." *Modelling and Simulation in Materials Science and Engineering* 4 (4): 371–396.

Hu, Yue, and PerKvols Heiselberg. 2018. "A New Ventilated Window with PCM Heat Exchanger – Performance Analysis and Design Optimization." *Energy and Buildings* 169: 185–194.

Ivshin, Y., and T. J. Pence. 1994. "A Constitutive Model for Hysteretic Phase Transition Behavior." *International Journal of Engineering Science* 32 (4): 681–704.

Kumarasamy, Karthikeyan, Jinliang An, Jinglei Yang, and En-Hua Yang. 2016. "Numerical Techniques to Model Conduction Dominant Phase Change Systems: A CFD Approach and Validation with DSC Curve." *Energy and Buildings* 118: 240–248.

Kumarasamy, Karthikeyan, Jinliang An, Jinglei Yang, and En-Hua Yang. 2017. "Novel CFD-Based Numerical Schemes for Conduction Dominant Encapsulated Phase Change Materials (EPCM) with Temperature Hysteresis for Thermal Energy Storage Applications." *Energy* 132: 31–40.

López Cárdenas, D. C., T. Barz, S. Körkel, and G. Wozny. 2015. "Nonlinear Ill-Posed Problem Analysis in Model-based Parameter Estimation and Experimental Design." *Computers & Chemical Engineering* 77: 24–42.

Manglik, Raj M., and Arthur E. Bergles. 1995. "Heat Transfer and Pressure Drop Correlations for the Rectangular Offset Strip Fin Compact Heat Exchanger." *Experimental Thermal and Fluid Science* 10 (2): 171–180.

Michel, Benoit, Patrick Glouannec, Adrien Fuentes, and Philippe Chauvelon. 2017. "Experimental and Numerical Study of Insulation Walls Containing a Composite Layer of PU-PCM and Dedicated to Refrigerated Vehicle." *Applied Thermal Engineering* 116: 382–391.

Moreles, E., G. Huelsz, and G. Barrios. 2018. "Hysteresis Effects on the Thermal Performance of Building Envelope PCM-walls." *Building Simulation* 11 (3): 519–531.

NIST/SEMATECH. 2015. "e-Handbook of Statistical Methods." January http://www.itl.nist.gov/div898/handbook/.

Noël, John A., Samer Kahwaji, Louis Desgrosseilliers, Dominic Groulx, and Mary Anne White. 2016. "Phase Change Materials." In *Storing Energy*, 249–272. New York: Elsevier.

NRGSIM. 2018. "NRGsim." October https://github.com/nrgsim/EnergyPlus-Fortran/tree/master/Documentation/EngRefMaterialPropertyPhaseChangeDualCurve.docx.

Rohsenow, Warren M., James P. Hartnett, and Young I. Cho. 1998. *Handbook of Heat Transfer*. New York: McGraw-Hill.

Rose, J., A. Lahme, N. U. Christensen, P. Heiselberg, M. Hansen, and K. Grau. 2009. "Numerical Method for Calculating Latent Heat Storage in Constructions Containing Phase Change Material." In *Proceedings of Building Simulation 2009: 11th Conference of the International Building Performance Simulation Association*, 400–407.

Rubitherm GmbH. 2018. "Data Sheets." August. https://www.rubitherm.eu/.

Shah, R. K., and D. P. Sekulic. 2003. *Fundamentals of Heat Exchanger Design*. Hoboken, NJ: Wiley.

Uzan, A. Y., Y. Kozak, Y. Korin, I. Harary, H. Mehling, and G. Ziskind. 2017. "A Novel Multi-dimensional Model for Solidification Process with Supercooling." *International Journal of Heat and Mass Transfer* 106: 91–102.

Vidi, S., H. Mehling, F. Hemberger, Th Haussmann, and A. Laube. 2015. "Round-Robin Test of Paraffin Phase-Change Material." *International Journal of Thermophysics* 36 (10-11): 2518–2522.

Virgone, Joseph, and Abdelkrim Trabelsi. 2016. "2D Conduction Simulation of a PCM Storage Coupled with a Heat Pump in a Ventilation System." *Applied Sciences* 6 (7): 193.

Voller, V. R., C. R. Swaminathan, and B. G. Thomas. 1990. "Fixed Grid Techniques for Phase Change Problems: A Review." *International Journal for Numerical Methods in Engineering* 30 (4): 875–898.

Ziskind, G. 2014. "Modelling of Heat Transfer in Phase Change Materials (PCMs) for Thermal Energy Storage Systems." In *Advances in Thermal Energy Storage Systems: Methods and Applications*, edited by Luisa F. Cabeza, 307–324. Woodhead Publishing Series in Energy. Cambridge: Elsevier Science.